Palaeogeography, Palaeoclimatology, Palaeoecology 649 (2024) 112335

Contents lists available at ScienceDirect

Palaeogeography, Palaeoclimatology, Palaeoecology

journal homepage: www.elsevier.com/locate/palaeo

Patterns of extinction and recovery across the Triassic–Jurassic boundary interval in three resilient Southern Tethyan carbonate platforms

Andrea Montanaro [a], Francesca Falzoni [b,*], Alessandro Iannace [c], Mariano Parente [c]

[a] SOCOTEC Italia, Via Annibale Zucchini 69, 44122 Ferrara, Italy
[b] Istituto di Geologia Ambientale e Geoingegneria, Consiglio Nazionale delle Ricerche, via Mario Bianco 9, 20131 Milan, Italy.
[c] Dipartimento di Scienze della Terra, dell'Ambiente e delle Risorse, Università degli Studi di Napoli Federico II, via vicinale cupa Cintia 21, 80126 Naples, Italy

ARTICLE INFO

Editor: L Angiolini

Keywords:
End-Triassic extinction
Dachstein-type carbonate platforms
Ocean acidification
Benthic foraminifera
Biostratigraphy
Carbon-isotope stratigraphy

ABSTRACT

During the end-Triassic extinction (ETE), carbonate platform biocalcifiers suffered high extinction rates that have been linked to volcanically-induced global changes in climate and carbon cycle. Most studies have been focused on the classical sections of the Northern Calcareous Alps (NCA, Austria) and Lombardy Basin (Italy), where the extinction of the aragonitic Dachstein-type biota (involutinid foraminifera and megalodontid bivalves) coincides with the demise of the carbonate platform and with the initial negative carbon isotope excursion (CIE) of the reference sections for the Triassic/Jurassic Boundary (TJB).

In this study, we present a detailed facies analysis, bio- and carbon-isotope stratigraphy of three Southern Tethyan carbonate platform sections, Mt. Messapion (Greece), Valle Agricola and Mt. Sparagio (southern Italy) that instead show persisting carbonate productivity across the TJB and potentially preserve the most detailed record of timing and patterns of the ETE in these ecosystems.

In the studied sections, the disappearance of the Dachstein-type biota is observed within a positive $\delta^{13}C_{carb}$ excursion that, according to our study, correlates with that documented in the Schattwald beds (NCA) and Malanotte Fm (Lombardy Basin) above the initial CIE. This level represents the true extinction of the Dachstein-type biota, while the disappearance in the Northern Tethyan sections of the NCA and Lombardy Basin represents a pseudoextinction coinciding with the carbonate platform demise. Above the ETE, Southern Tethyan carbonate platform sections are characterized either by microbial laminites or ooid and oncoid limestones and low-diversity associations.

This study reveals a possible paleogeographic and/or latitudinal control on the response of biocalcifiers and carbonate platform ecosystems during the ETE. The Dachstein-type biota was resilient to the environmental perturbations associated with the initial CIE in Southern Tethys, but probably failed to survive subsequent and/or prolonged stress. Despite extinctions, Southern Tethyan carbonate platforms adapted to environmental disturbances through a shift of the dominant carbonate production style from aragonitic biocalcification to chemical and microbially-mediated $CaCO_3$ precipitation. The ecosystem recovery was slow and aragonitic biocalcifiers (dasycladacean algae) reappeared during the early Sinemurian.

1. Introduction

The end-Triassic extinction (ETE) is one of the five biggest extinctions of the Phanerozoic (Raup and Sepkoski, 1982) and it resulted in a severe drop in biodiversity in the marine and continental realms (Hallam and Wignall, 1997; Hallam, 2002). Massive volcanism of the Central Atlantic Magmatic Province (CAMP), which represents the most extensive continental Large Igneous Province known on Earth, has been implied as a possible cause of the ETE, based on radiochronologic ages documenting that its activity straddles the Triassic–Jurassic boundary (TJB) interval (Marzoli et al., 1999, 2018; Deenen et al., 2010; Blackburn et al., 2013; Bond and Wignall, 2014; Dal Corso et al., 2014).

Despite many studies published in the last two decades (see Wignall and Atkinson, 2020 and Schoepfer et al., 2022, for recent reviews), several open questions remain about the timing and causes of the ETE. In the marine realm, a wealth of data has been gathered from stratigraphic sections representative of deep-water hemipelagic and pelagic environments, while much less is known about the record of the ETE in

* Corresponding author.
E-mail address: francesca.falzoni@cnr.it (F. Falzoni).

https://doi.org/10.1016/j.palaeo.2024.112335
Received 22 January 2024; Received in revised form 4 June 2024; Accepted 12 June 2024
Available online 15 June 2024

carbonate platforms.

In many areas of the Tethys Ocean, carbonate platform sedimentation was terminated around the TJB. Classical examples of this pattern are found in the Northern Calcareous Alps (NCA, Austria: Gaździcki et al., 1979; Felber et al., 2015) and in the Transdanubian Range (Hungary: Pálfy et al., 2021). In these localities, Upper Triassic Dachstein-type carbonate platforms were dominated by scleractinian corals and calcareous sponges in reef habitats, and by megalodontid bivalves, involutinid benthic foraminifera and dasycladacean algae in backreef lagoons (Flügel, 1981; Schäfer and Senowbari-Daryan, 1981; Flügel and Senowbari-Daryan, 2001; Bernecker, 2005; Krystyn et al., 2005; Felber et al., 2015; Mette et al., 2016). The demise of this rich and diverse biota has been associated with ocean acidification caused by the massive injection of carbon dioxide in the ocean-atmosphere system by CAMP volcanic activity (Hautmann, 2004; Kiessling and Simpson, 2011; Greene et al., 2012; Hönisch et al., 2012; Martindale et al., 2012). Platform top sections in the NCA record a long gap between the Rhaetian Oberrhaet Limestone and the Hettangian to Sinemurian Hierlatz Limestone and Adnet Fm (Krystyn et al., 2005). This gap has been related to a rapid sea-level drop (up to nearly 150 m) at the top of the Oberrhaet Limestone, followed by a slow transgressive phase that temporarily interrupted carbonate platform productivity during the TJB interval (Krystyn et al., 2005). More complete TJB sections are restricted to the intraplatform Eiberg Basin, where the extinction of the Rhaetian biota coincides with a switch from the limestones of the Kössen Fm to the carbonate-poor sediments of the lowermost Kendelbach Fm (Schattwald beds) (e.g., the Löruns section: McRoberts et al., 2012; Felber et al., 2015). A significant hiatus is implied in sections where the Löruns oolite directly overlies the Kössen Fm (e.g., Steinernes Meer: Felber et al., 2015). In the Transdanubian Range, the demise of the Dachstein-type carbonate platform and the extinction of its biota is associated with a significant hiatus across the TJB, which was attributed to emersion followed by a tectonically-driven platform drowning event, and more recently to a switch to a submarine erosion regime coinciding with the transformation from the rimmed Dachstein platform to a carbonate ramp (Pálfy et al., 2021, and papers cited therein).

The classical sections of the Lombardy Basin (southern Alps, northern Italy) show a pattern very similar to the Löruns section (NCA, Austria), with the extinction of the Upper Triassic shallow-water benthic calcifiers coinciding with the interruption of the carbonate platform

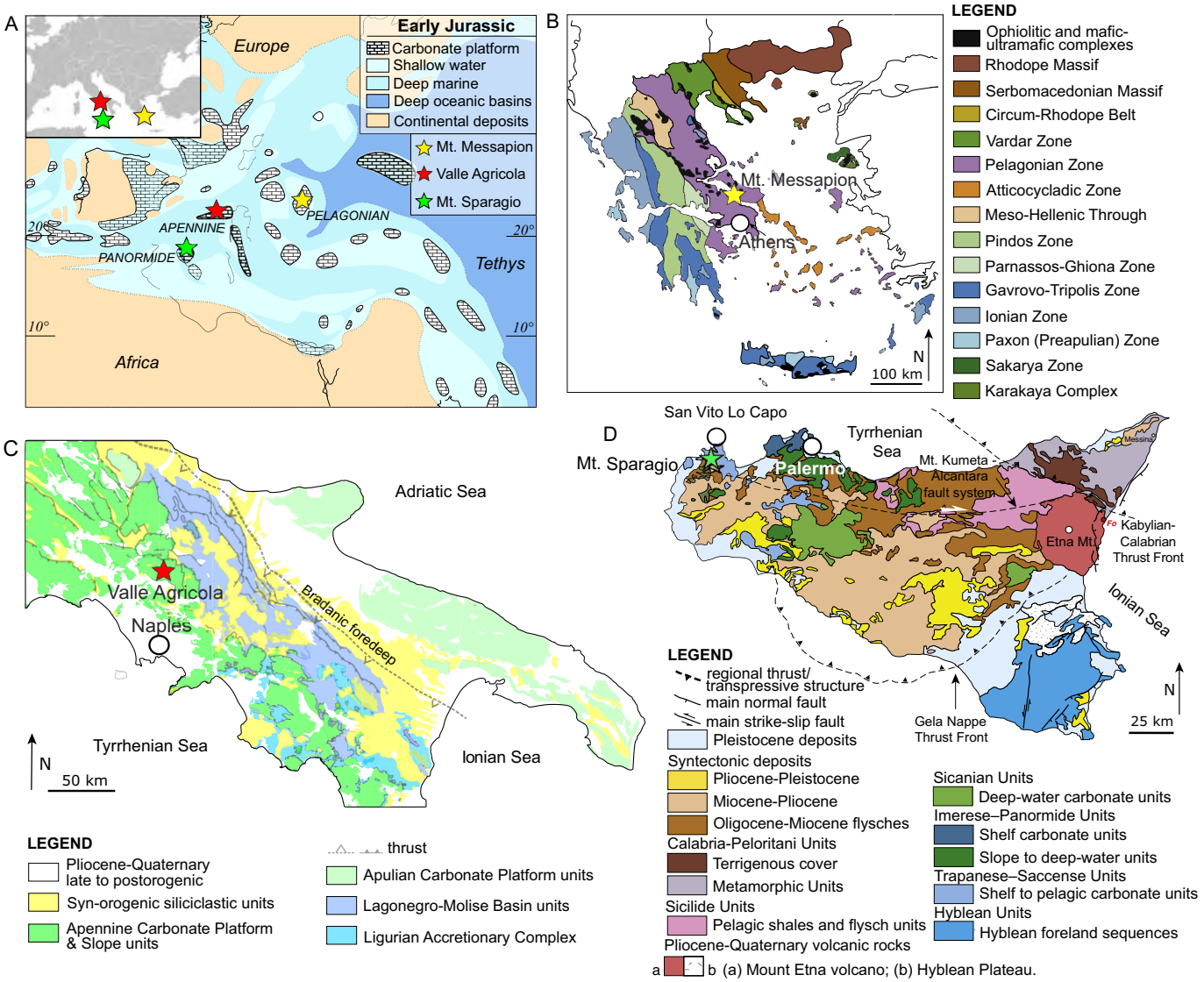

Fig. 1. (A) Paleogeographic map for the Early Jurassic of the Tethys, with location of the three studied sections (modified from Dercourt et al., 2000); (B) schematic geological map of Greece (modified from Koglin et al., 2009); (C) schematic geological map of Southern Apennines (modified from Tavani et al., 2021); (D) schematic geological map of Sicily (modified from Tassi et al., 2012).

productivity at the boundary between the Calcare di Zu and the Malanotte Fm (Galli et al., 2005, 2007).

Only a few carbonate platforms worldwide were apparently able to survive the crisis at the end of the Triassic. In these resilient carbonate platforms, fossiliferous Upper Triassic limestones with corals, sponges, chaetetids, large megalodontid bivalves and rich benthic foraminiferal associations change abruptly into unfossiliferous peritidal and/or ooid-oncoid limestones around the TJB. This pattern is well represented by the carbonate platforms in southern Italy (Mancinelli et al., 2005; Todaro et al., 2017, 2018, 2022), Greece (Romano et al., 2008), Western Turkey (Coskun Tunaboylu et al., 2014), and United Arab Emirates (Maurer et al., 2008; Al-Suwaidi et al., 2016; Ge et al., 2018; Urban et al., 2023). The study of these resilient carbonate platforms is of great interest because they preserve the most detailed record of biotic changes during the ETE in shallow-water tropical ecosystems.

In this paper, we present sedimentological, biostratigraphic and stable isotope ($\delta^{13}C_{carb}$ and $\delta^{18}O_{carb}$) data for three carbonate platform sections that show neither a significant gap nor a switch to carbonate-poor facies across the TJB: 1) Mt. Messapion (Pelagonian Carbonate Platform, Greece), 2) Valle Agricola (Apennine Carbonate Platform, Campania, southern Italy) and 3) Mt. Sparagio (Panormide Carbonate Platform, Sicily, southern Italy). These three sections were located at subtropical latitudes in the south-western Tethys Ocean during the Late Triassic–Early Jurassic (Fig. 1A). We describe the record of biotic changes across the TJB and we discuss the chronostratigraphic calibration of the most important bioevents. In addition, we discuss the reliability of the carbon-isotope record and we tentatively trace a bio- and carbon-isotope correlation between Southern Tethyan carbonate platforms and the classical sections of the Lombardy Basin and NCA.

2. Materials and methods

2.1. The studied sections, microfacies analysis, and biostratigraphy

2.1.1. Mt. Messapion (Greece)

The Mt. Messapion section (geographic coordinates: 38°27′44.31"N, 23°28′43.08″E) is located in Greece, 10 km west of the city of Halkida (or Chalkida), and about 60 km to the north-west of Athens (Fig. 1B). It was part of the Pelagonian Carbonate Platform, which was established in the Middle Triassic and dismembered and drowned starting from the Early Jurassic (Celet et al., 1988; Haas et al., 2009) (Fig. 1A). The Upper Triassic–Lower Jurassic platform carbonates exposed in the Mt. Messapion section display m-thick shallowing upward peritidal cycles, with subtidal facies capped by microbial laminites and paleosols. Facies, peritidal cyclicity and biostratigraphy of this section were studied by Romano et al. (2008).

The 293 m-thick Mt. Messapion section was logged at decimeter to meter scale along a road cut on the southern slope of the mountain. Field observations were integrated with microfacies and biostratigraphic analyses carried out on 188 thin sections.

2.1.2. Valle Agricola (Italy)

The Valle Agricola section (geographic coordinates: 41°25′42.97"N, 14°14′39.22″E) is located near the village of Valle Agricola (Matese Mountains, Campania, southern Italy) (Fig. 1C). It was part of the Apennine Carbonate Platform, which was established in the Late Triassic at the north-western margin of the Adria promontory (Fig. 1A) and persisted, with short interruptions of sedimentation, until the Late Cretaceous, when it was terminated by emersion (D'Argenio and Alvarez, 1980; Bernoulli, 2001; Bosellini, 2004; Parente et al., 2022). The Valle Agricola section consists of Upper Triassic peritidal limestones with megalodontids, corals and chaetetids, overlain by Lower Jurassic ooid-oncoid limestones. The section described in this paper corresponds to the lower part of the Costa dei Frascari section of Mancinelli et al. (2005).

The 245 m-thick Valle Agricola section was logged in the field at decimeter to meter scale. The outcrop is accessible along a mountain path that offers a nearly continuous high-quality exposure of fresh rock surfaces with the exception of an interval in the upper part of the section where the outcrop is discontinuous or covered by vegetation and small-scale faults slightly offset the beds. Field observations were integrated with microfacies and biostratigraphic analyses on 196 thin sections.

2.1.3. Monte Sparagio (Italy)

The Mt. Sparagio section (geographic coordinates: 38°3′47.36"N, 12°43′13.32″E) is located near the village of Custonaci (northwestern Sicily, southern Italy), in the southern part of the San Vito Lo Capo Peninsula (Fig. 1D). It was part of the Panormide Carbonate Platform connecting Africa and Adria along the southwestern arm of the Tethys Ocean (Zarcone et al., 2010) (Fig. 1A). The section records peritidal carbonate sedimentation in the inner sector of the carbonate platform during the Late Triassic (Sciacca Fm) to the Early Jurassic (Inici Fm), followed by drowning in the Middle Jurassic (Rosso Ammonitico Fm). Data on the litho- and biostratigraphy, facies, and carbon- and strontium-isotope stratigraphy can be found in Todaro et al. (2017, 2018, 2022).

The 250 m-thick Mt. Sparagio section was logged in the field at decimeter to meter scale. Field observations were integrated with microfacies and biostratigraphic analyses on 199 thin sections.

2.2. Carbon and oxygen stable isotope analysis

Carbonate powders for stable isotope analysis were sampled in the field, using a battery-operated hammer drill equipped with carbide-tungsten bits of diameter ranging from 10 to 18 mm. About 10 to 20 g of powder per sample were produced by drilling a 5–10 cm deep hole after eliminating the altered surface of the rock and avoiding cement-filled fractures and cavities and recrystallized shell fragments. This sampling methodology for stable isotope analysis has been already applied to other carbonate platform sections (e.g., Franceschi et al., 2014; Eltom et al., 2021) but we further tested its reliability by comparing the stable isotope values obtained from selected microdrilled polished slabs and bulk samples drilled in the field in the same bed. Further details are provided in the supplementary material (File S1).

Carbonate powders of the Mt. Messapion (321 samples, sampling resolution from 20 cm to 4.2 m across outcrop gaps) and Mt. Sparagio sections (221 samples, sampling resolution from 20 cm to 4.3 m across outcrop gaps) were analyzed for carbon ($\delta^{13}C_{carb}$) and oxygen ($\delta^{18}O_{carb}$) isotope ratios at the Laboratory of Paleoclimatology and Isotopic Stratigraphy of the Department of Physics and Earth Sciences of the University of Ferrara (Italy). Carbonate powders of the Valle Agricola section (550 samples, sampling resolution from 10 cm to 6.7 m across outcrop gaps) were analyzed at the Department of Earth Science "A. Desio", University of Milan (Italy). The results are reported as per mil (‰) deviation relative to the Vienna-Pee Dee Formation Belemnite (VPDB) international standard. Details on the analytical techniques are given in the supplementary material (File S1).

2.3. Repository of the studied material

All the samples and thin sections used for this study are stored at the Dipartimento di Scienze della Terra, dell'Ambiente e delle Risorse, Università degli Studi di Napoli Federico II, collection Mariano Parente.

3. Results

In the studied sections, lithofacies were recognized based on texture, main components and sedimentary structures. Lithofacies descriptions and interpretations are summarized in Tables 1–3. Detailed lithofacies descriptions, outcrop and microfacies photographs are given in the Supplementary material (File S1). Stable isotope results are included in the supplementary material (File S2). Notes on the identification of

foraminifera and the author(s) and year of the description of the genera and species mentioned in the text and/or figures are given in the taxonomic appendix (Appendix A).

3.1. Mt. Messapion

3.1.1. Lithofacies, fossil associations and bioevents

Ten lithofacies are recognized in the Mt. Messapion section (Table 1; File S1). The section is subdivided into three intervals, based on fossil content and dominant lithofacies (Fig. 2).

Interval A (0–52.7 m) is characterized by peritidal cycles generally capped by red paleosols. Macrofossil associations are represented by large (up to 40 cm) dicerocardiid and megalodontid bivalves, and by gastropods. Microfossil associations comprise dasycladacean algae and rich benthic foraminiferal assemblages dominated by involutinids. The most common involutinid taxa are: *Triasina hantkeni* (Fig. 3A), *Aulotortus* spp. (Fig. 3B-D), *Parvalamella friedli*, *Lamelliconus permodiscoides*, *Frentzenella crassa* and *Trocholina* spp. (Fig. 3E). Lageninids, possibly falling in the range of variability of the genera *Polarisella* (Fig. 3F) and *Austrocolomia*, in addition to *Gandinella falsofriedli*, *Glomospira* sp., (Fig. 3G), undetermined textulariinids (Fig. 3H), and to the fusulinid genus *Endoteba* (Fig. 3I) are represented by rare specimens. Robertininids (family Duostominidae: Fig. 3J) and miliolinids (family Milioliporidae) are rare and observed in few samples. Dasycladacean algae are common in some samples and are mainly represented by *Griphoporella curvata* (Fig. 3K). The incertae sedis *Thaumatoporella parvovesiculifera* is common in few samples. Ostracods and cyanophyceans occur in mud-rich and laminated microfacies.

The uppermost bed with megalodontid bivalves occurs at 51.4 m, very close to the top of interval A. The highest occurrence (HO) of *Triasina hantkeni*, of other involutinid genera (*Aulotortus*, *Lamelliconus*, and *Parvalamella*), of the family Duostominidae, and of the dasycladacean alga *G. curvata* marks the top of interval A at 52.7 m.

Interval B (52.7–125.7 m) is characterized by peritidal cycles with dm-thick intervals of laminated whitish dolomites. Red paleosols are present only in the basal 15 m. This interval is poorly fossiliferous. Macrofossils are very rare and represented by fragments of small bivalves. Microfossil associations are dominated by *T. parvovesiculifera* (Fig. 3L); textulariinid benthic foraminifera (Fig. 3M-N) and ostracods are very rare.

Interval C (125.7–293 m) is characterized by peritidal cycles with cm- to dm-thick intervals of laminated whitish dolomites. Red paleosols are especially frequent in the uppermost part of the interval. Oncoids and ooids are frequent components of grainy facies. This interval is more fossiliferous, compared to interval B, especially in its upper part. Macrofossil associations are characterized by bivalves and gastropods. Microfossil associations comprise foraminiferal assemblages with moderate diversity dominated by textulariinids and mainly represented by *Duotaxis birmanica* (Fig. 3O), *Duotaxis metula*, *Siphovalvulina* spp. (Fig. 3P), *Radoicicina ciarapicae* (Fig. 3Q). *Everticyclammina* sp. (Fig. 3R) occurs from 214.4 m. Poorly preserved dasycladacean fragments occur starting from 192.8 m. The lowest occurrence (LO) of specimens referable with certainty to *Palaeodasycladus mediterraneus* (Fig. 3S-T) is at 224.5 m. *Thaumatoporella parvovesiculifera* is relatively less common compared to interval B.

3.1.2. Carbon and oxygen stable isotopes

The $\delta^{13}C_{carb}$ values range overall between −1 and +2.8‰ with most values between +1 and +2.5‰ (Fig. 2). The carbon isotope profile shows some high-amplitude fluctuations of up to 2–3‰ over short stratigraphic intervals <2–3 m thick, especially between 0 and 140 m. These high-amplitude/short-term fluctuations are superimposed on larger scale features, which develop over intervals 40 to 100 m thick. The first large-scale feature is a positive excursion reaching a maximum of +2.7‰ at about 20 m and ending at a minimum of about +0.4‰ at 42 m. A second large-scale positive excursion starts with a steep rise to a value of +2.4‰ at 44.7 m and then peaks to +2.7‰ at 59 m. From this maximum, $\delta^{13}C_{carb}$ values show a long-term decrease to a minimum of −1‰ at 137.6 m. Above this level, the $\delta^{13}C_{carb}$ is characterized by a third broad positive excursion with values fluctuating around +2‰.

The $\delta^{18}O_{carb}$ values range overall between −7.1 and −0.6‰ with most values between −4 and −1.5‰ (Fig. 2). The oxygen isotope profile

Table 1
Lithofacies of the Mt. Messapion section. Relative abundances given as number of specimens/abiotic grains per thin section as follows: vr (very rare) = 1; r (rare) = 2–3; f (frequent) = 4–10; c (common) 10–25; vc (very common) = 25–50; a (abundant) > 50.

Mt. Messapion				
Lithofacies	Texture	Abiotic components	Fossil content	Depositional environment
Megalodontid floatstone (Fb)	Floatstone in mudstone-wackestone matrix	Peloids (f)	Bivalves (a), matrix: foraminifera (c) and dasycladaceans (c), ostracods (r), *T. parvovesiculifera* (vr), gastropods (r)	Subtidal lagoon
Bioclastic mudstone-wackestone (MWb)	Mudstone-wackestone	Intraclasts (r)	Bivalve fragments (c), foraminifera (c) and dasycladaceans (c), gastropods (r), nodules of cyanophyceans (r), echinoid spines (r), ostracods (r), *T. parvovesiculifera* (r)	Subtidal lagoon
Oncoid floatstone (Fo)	Floatstone in mudstone matrix	Oncoids (a), concentric ooids (f), intraclasts (r), peloids (c)	Foraminifera (vr), dasycladaceans (vr)	Subtidal lagoon
Ooid packstone-grainstone (PGo)	Packstone-grainstone	Ooids (a), intraclasts (r)	Gastropods (r), bivalve fragments (r), *T. parvovesiculifera* (r), foraminifera (r-f)	Inlet of tidal channels (subtidal)
Homogeneous mudstone (M)	Mudstone	Intraclasts (r)	Foraminifera (r), ostracods (r), *T. parvovesiculifera* (r-c)	Subtidal lagoon
Peloidal and bioclastic packstone-grainstone (PGpb)	Packstone-grainstone	Peloids (a), intraclasts (r-f), oncoids (vr)	Bivalve fragments (vr-a), foraminifera (vr-a) and dasycladaceans (vr-a), gastropods (r-f), cyanophyceans (r), echinoid spines (r), *T. parvovesiculifera* (r-f)	Subtidal lagoon
Flat pebble conglomerate (fp)	Rudstone	Lithoclasts (a), black pebbles (f)	Ostracods (vr)	Tidal flat (intertidal)
Fenestral mudstone-wackestone (MWf)	Mudstone-wackestone	Intraclasts (c), black pebbles (c)	*T. parvovesiculifera* (c), foraminifera (vr-r), ostracods (r-f)	Tidal flat (intertidal)
Microbial laminite (LAM)	Bindstone	Intraclasts (c), black pebbles (c)	Foraminifera (r), bivalve fragments (vr), ostracods (vr), *T. parvovesiculifera* (r)	Tidal flat (intertidal-supratidal)
Paleosol (PAL)	Mudstone	Intraclasts (c), lithoclasts (c)	Barren (reworked foraminifera, ostracods, bivalves and dasycladaceans)	Subaerial

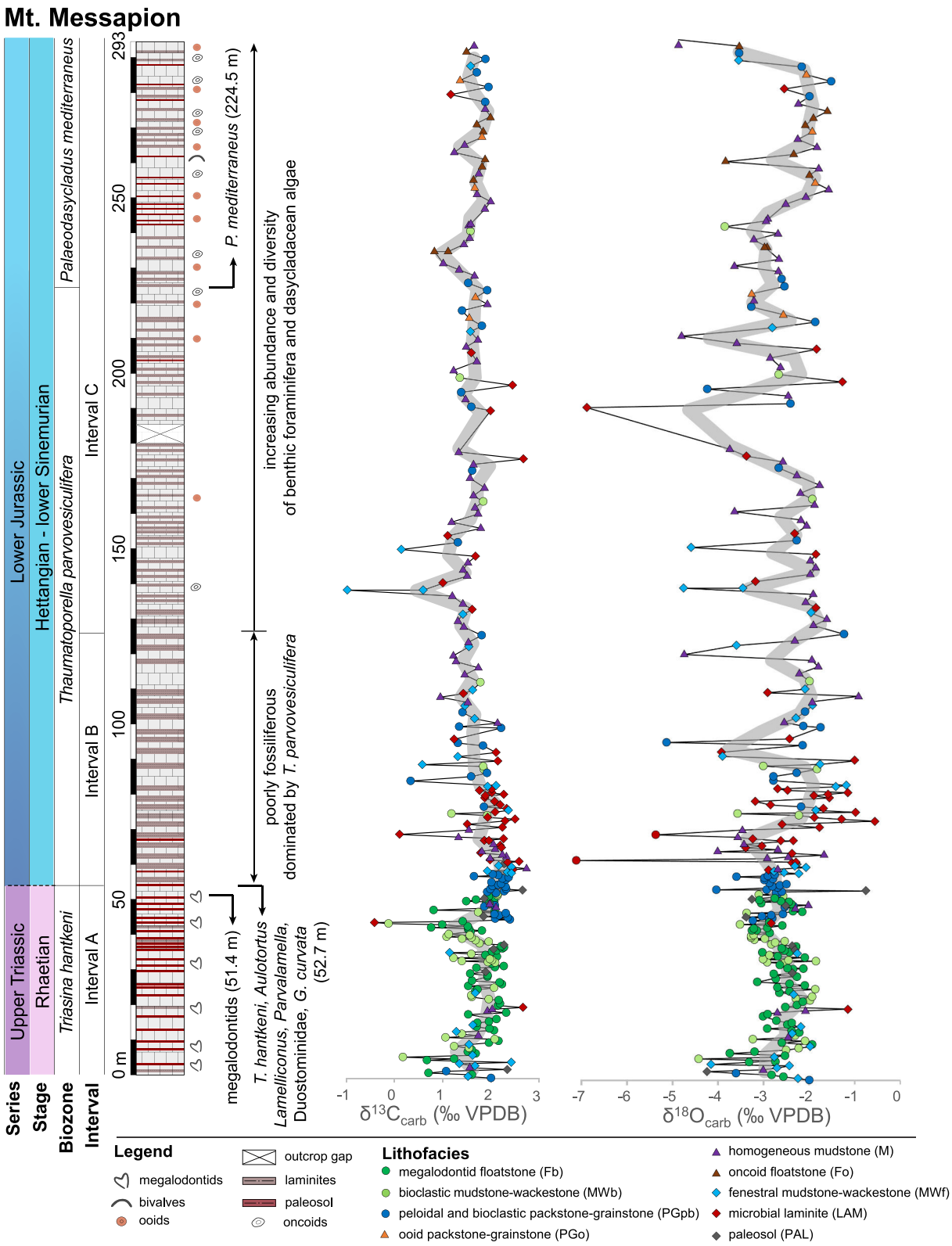

Fig. 2. Litho-, biostratigraphy and stable isotope profiles ($\delta^{13}C_{carb}$ and $\delta^{18}O_{carb}$) of the Mt. Messapion section (Pelagonian Carbonate Platform, Greece). Interval A is fossil-rich and its top is defined by the extinction of the benthic foraminifera *Triasina hantkeni*, *Aulotortus* spp., *Lamelliconus* spp., *Parvalamella* spp., of the Duostominidae, and of the dasycladacean alga *Griphoporella curvata*. Interval B is poorly fossiliferous and dominated by *Thaumatoporella parvovesiculifera*. The top of interval B is defined by the onset of increasing abundance and diversity of benthic foraminifera followed by that of dasycladacean algae (see text for further details). The Triassic/Jurassic boundary is approximated to the extinction level of the *T. hantkeni* assemblage (see paragraph 4.2). The gray line in the stable isotope profiles represents a 5 m moving average.

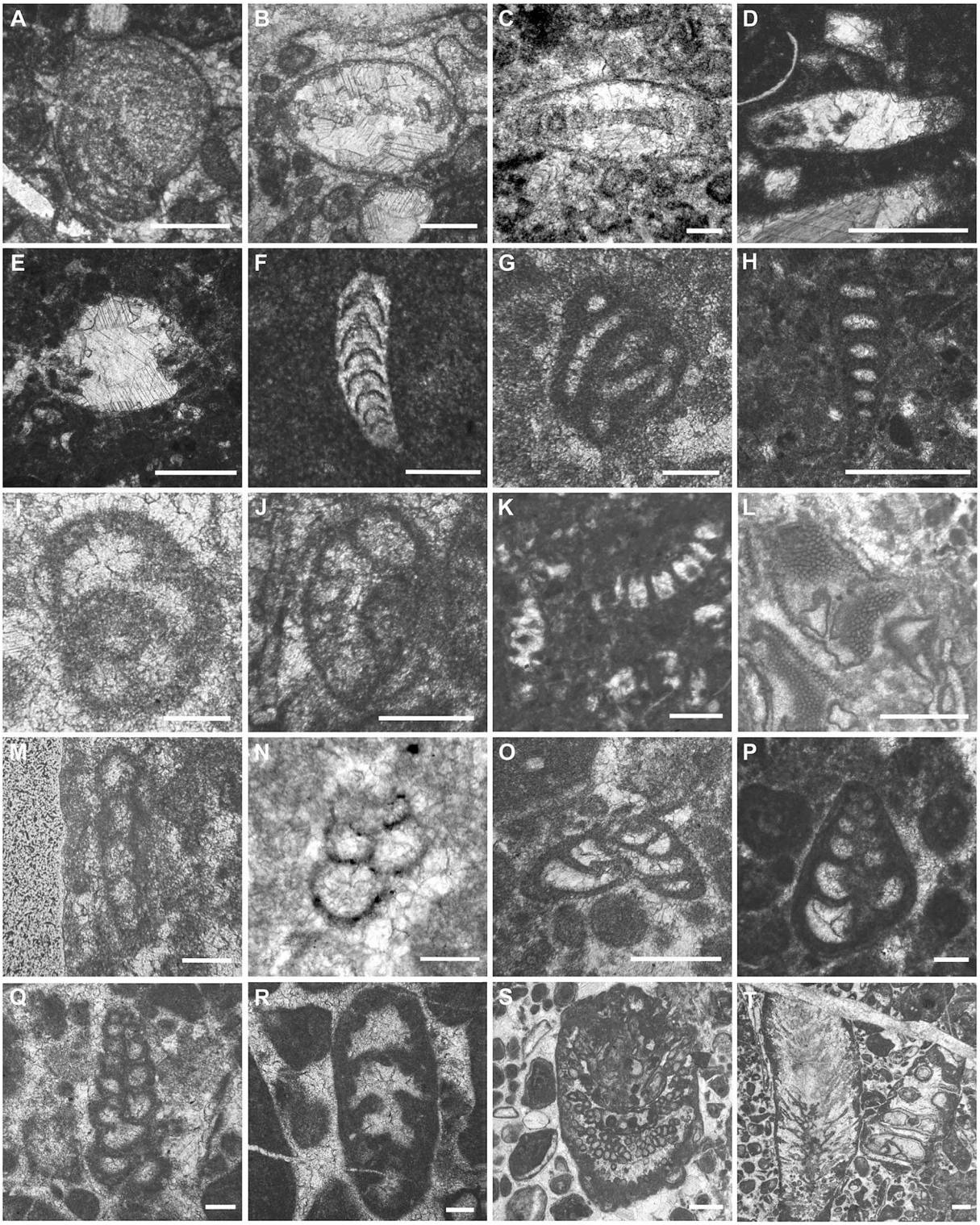

Fig. 3. Microfossils of the Mt. Messapion section. A) *Triasina hantkeni* (52.7 m); B) *Aulotortus sinuosus* (52.7 m); C) *Aulotortus communis* (38.3 m); D) *Aulotortus tumidus* (35.9 m); E) *Trocholina* sp. (5.8 m); F) *Polarisella* sp. (8.1 m); G) *Glomospira* sp. (47.1 m); H) undetermined textulariinid (5.8 m); I) *Endoteba* sp. (38.3 m); J) Duostominidae (52.7 m); K) *Griphoporella curvata* (17.5 m); L) *Thaumatoporella parvovesiculifera* (116.5 m); M) cf. *Endotriadella* sp. (53.0 m); N) ?*Siphovalvulina* (60.5 m); O) *Duotaxis birmanica* (256.5 m); P) *Siphovalvulina* cf. *colomi* (268.9 m); Q) *Radoicicina ciarapicae* (239.7 m); R) *Everticyclammina* sp. (239.7 m); S) *Palaeodasycladus mediterraneus* (232.9 m); T) *Palaeodasycladus mediterraneus* (239.7 m). Scale bar is 500 μm for photographs A-B, D-E, H, L, S-T; it is 200 μm for photograph J; it is 100 μm for photographs C, F-G, I, M-R. Numbers in parentheses refer to height from the base of the section.

shows some high-amplitude/short-term fluctuations up to 5‰ over 2 m-thick stratigraphic intervals that are particularly common above 50 m. These fluctuations are superimposed on large scale features. A first positive excursion lies between 0 and 42 m, and reaches a maximum of −1.1‰ at 20 m; a second positive excursion lies between 42 and 68.7 m, where the $\delta^{18}O_{carb}$ values rise to −0.75‰ at 55 m; a third positive excursion lies between 68.7 and 90.6 m, where the $\delta^{18}O_{carb}$ values rise to −0.56‰ at 72.5 m. The overlying stratigraphic interval is characterized by frequent high-amplitude fluctuations superimposed on a relatively stable long-term trend with values around −2.5‰. The uppermost part of the section (279.3 to 291 m) is characterized by a decreasing trend to −4.8‰.

3.2. Valle Agricola

3.2.1. Lithofacies, fossil associations and bioevents

Nine lithofacies are recognized in the Valle Agricola section (Table 2; File S1). The section is subdivided into two intervals, based on fossil content and dominant lithofacies (Fig. 4).

Interval A (0–211.6 m) is made of peritidal cycles with rich and diverse macrofossil associations, consisting mainly of megalodontid bivalves, chaetetids, and corals, testifying deposition in a sector close to the platform margin. The microfossil content is also rich and diverse and dominated by benthic foraminifera, associated with common dasycladacean algae (mainly represented by fragments referable to *Griphoporella curvata*) and *T. parvovesiculifera*. Among foraminifera, the most significant taxa are: *Aulotortus* spp. (Fig. 5A-B), *Aulosina oberhauseri* (at the base of the section; Fig. 5C), *Triasina hantkeni* (from 23.0 m; Fig. 5D-E), *Parvalamella friedli* (Fig. 5F), *Lamelliconus permodiscoides* (Fig. 5G), *Frentzenella crassa* (Fig. 5H) and *Trocholina* spp. (Fig. 5I). Lageninids, tentatively referable to the genera *Polarisella* and *Austrocolomia* (Fig. 5J), are represented by rare specimens. Textulariinids assigned to "*Trochammina*" spp. (Fig. 5K-L), *Duotaxis metula* (Fig. 5M) and *D. birmanica*, "*Tetrataxis*" spp., in addition to *Gandinella falsofriedli* (Fig. 5N), and *Glomospira* sp. are common. Rare specimens belonging to the fusulinid genus *Endoteba* (Fig. 5O), to miliolinids of the family Milioliporidae (Fig. 5P) and Ophthalmidiidae (Fig. 5Q), and to robertininids of the family Duostominidae (Fig. 5R-T) are also present.

The LO of *T. hantkeni* is identified at 23.0 m (Fig. 4) in the lower part of interval A, about 100 m below the level indicated by the lower-resolution study of Mancinelli et al. (2005). The uppermost beds with megalodontid bivalves, and fragments of corals and chaetetids are observed at 196.5 m, 200 m, and 201.2 m, respectively. The HO of *T. hantkeni*, of other involutinid genera (*Aulotortus*, *Lamelliconus*, and *Parvalamella*), of the family Duostominidae, and of *G. curvata* is observed at 211.6 m and marks the top of interval A.

The uppermost part of interval A is characterized by discontinuous exposure and by the occurrence of small-scale faults. However, the outcrop is continuous, and no faults were observed at the boundary between interval A and B, which is traced within the same bed.

Interval B (211.6–245 m) consists of ooid packstone-grainstone at the base and of oncoid grainstone-rudstone in the upper part. It is unfossiliferous (samples at 212, 212.2 and 212.5 m are barren) to very poorly fossiliferous up to 217.3 m. The diversity and abundance of micro- and macrofossils gradually increase toward the top of the section, where cyanophycean nodules, gastropods and fragments of bivalves represent the dominant biotic components, accompanied by rare textulariinid benthic foraminifera ("*Trochammina*" species, ?*Siphovalvulina*) and echinoid spines in some samples.

3.2.2. Carbon and oxygen stable isotopes

The $\delta^{13}C_{carb}$ values range overall between −1.4 and +3.5‰ and most values fall between +1 and +3‰ (Fig. 4). The carbon isotope profile shows several high-amplitude fluctuations, of up to 2–3‰ over short stratigraphic intervals <2–3 m thick, superimposed on larger scale features that develop over intervals 20 to 100 m thick. The first positive excursion is observed between 0 and 20 m, and reaches a maximum of +2.9‰ at 7 m. A second positive excursion lies between 20 and 57 m, and reaches a maximum of +3‰ at 35 m. At 58.5 m, the $\delta^{13}C_{carb}$ rises sharply to +2.8‰ followed by a gradual decrease to a minimum of +1.2‰ at 120 m. From 120 to 193 m, the $\delta^{13}C_{carb}$ record shows frequent high-amplitude (2–4‰) meter scale fluctuations around average values of about +1.3‰ that are superimposed on a slight long-term decreasing trend. The top of the section (193–245 m) shows the largest-scale positive excursion, which is characterized by a two-step rise to a maximum value of +3.5‰ reached at 214.9 m and followed by a gradual decrease to +2.5‰. This interval is characterized by the absence of high-frequency fluctuations in the $\delta^{13}C_{carb}$ record.

Table 2
Lithofacies of the Valle Agricola section. Relative abundances given as number of specimens/abiotic grains per thin section as follows: vr (very rare) = 1; r (rare) = 2–3; f (frequent) = 4–10; c (common) 10–25; vc (very common) = 25–50; a (abundant) > 50.

Valle Agricola				
Lithofacies	Texture	Abiotic components	Fossil content	Depositional environment
Fossiliferous floatstone (Ff)	Floatstone in wackestone- packstone matrix	Peloids (f), black pebbles (r)	Bivalves (a), corals (f), chaetetids (f) matrix: foraminifera (f-c) and dasycladaceans (c), *T. parvovesiculifera* (r-c), ostracods (r), gastropods (c)	Subtidal lagoon
Bioclastic mudstone-wackestone (MWb)	Mudstone-wackestone	Intraclasts (r)	Bivalve fragments (f-c), foraminifera (f-c) and dasycladaceans (r-c), gastropods (r), cyanophyceans (r), echinoid spines (r), *T. parvovesiculifera* (r-a)	Subtidal lagoon
Homogeneous mudstone (M)	Mudstone	Intraclasts (r)	Foraminifera (r)	Subtidal lagoon
Peloidal and bioclastic wackestone-packstone (WPpb)	Wackestone-packstone	Peloids (a), intraclasts (r), oncoids (vr)	Bivalve fragments (c), foraminifera (c-a) and dasycladaceans (f), gastropods (f), cyanophyceans (r), echinoid spines (r), ostracods (r), *T. parvovesiculifera* (r-a)	Subtidal lagoon
Oncoid grainstone-rudstone (GRo)	Grainstone-rudstone	Oncoids (a), ooids (r-f), intraclasts (vr), peloids (c)	Gastropods (r-c), bivalve fragments (r-c), echinoid spines (r), foraminifera (r)	Platform margin-sand shoal (intertidal)
Ooid packstone-grainstone (PGo)	Packstone-grainstone	Ooids (a), intraclasts (r), peloids (r), oncoids (r)	Foraminifera (r), echinoid spines (r), ostracods (r)	Platform margin-sand shoal (intertidal)
Fenestral mudstone-wackestone (MWf)	Mudstone-wackestone	Intraclasts (vr), black pebbles (c)	*T. parvovesiculifera* (c), foraminifera (r), ostracods (r), bivalve fragments (r)	Tidal flat (intertidal)
Microbial laminite (LAM)	Bindstone-mudstone	Intraclasts (c), black pebbles (c)	Foraminifera (r), ostracods (r), gastropods (r), *T. parvovesiculifera* (r), bivalve fragments (r)	Tidal flat (intertidal-supratidal)
Lithoclastic-intraclastic breccia (B)	Rudstone	Lithoclasts (a), intraclasts (a)	Bioclasts (r)	Tidal flat (intertidal-supratidal)

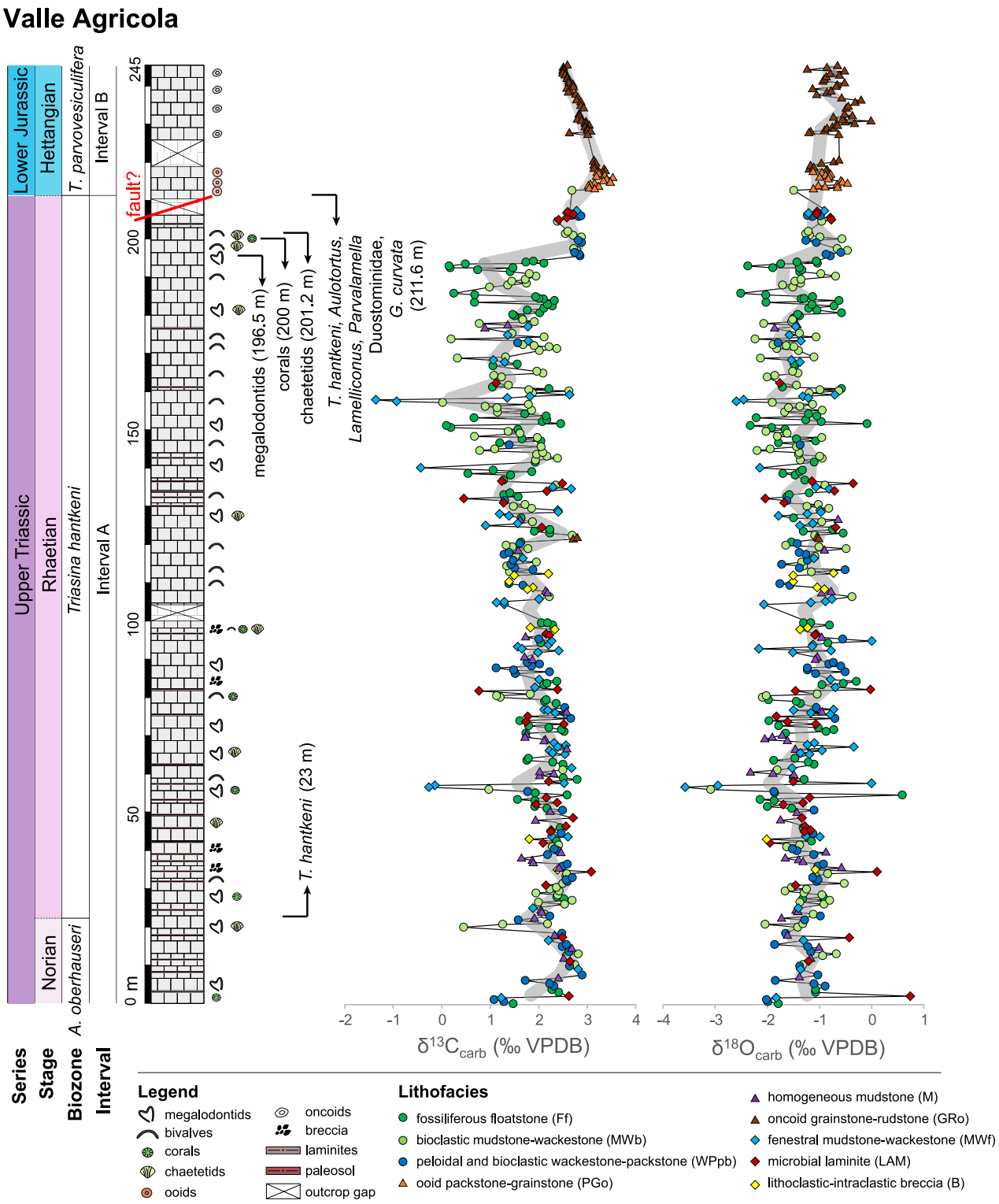

Fig. 4. Litho-, biostratigraphy and stable isotope profiles ($\delta^{13}C_{carb}$ and $\delta^{18}O_{carb}$) of the Valle Agricola section (Apennine Carbonate Platform, Campania, Italy). Interval A is fossil-rich and its top is defined by the extinction of the benthic foraminifera *Triasina hantkeni*, *Aulotortus* spp., *Lamelliconus* spp., *Parvalamella* spp., of the Duostominidae, and of the dasycladacean alga *Griphoporella curvata*. Interval B is poorly fossiliferous and contains gastropods and rare textulariinid benthic foraminifera (see text for further details). The Triassic/Jurassic boundary is approximated to the extinction level of the *T. hantkeni* assemblage (see paragraph 4.2). The gray line in the stable isotope profiles represents a 5 m moving average.

The $\delta^{18}O_{carb}$ values of the samples from the Valle Agricola section range overall between −3.6 and +0.7‰ with most values between −2 and 0‰ (Fig. 4). The oxygen isotope profile shows high- amplitude fluctuations of up to 2–3‰ from 0 to 193 m, and up to 1‰ from 193 m to the top of the section. These fluctuations extend over stratigraphic intervals that are 2–3 m thick. Although less clear than the carbon isotope record, the oxygen record also shows large-scale features. A first positive excursion occurs between 0 and 56.5 m, and reaches a maximum of +0.1‰ at 34.5 m. A second broad positive excursion is observed between 56.5 m and 156.8 m, where the $\delta^{18}O_{carb}$ reaches a

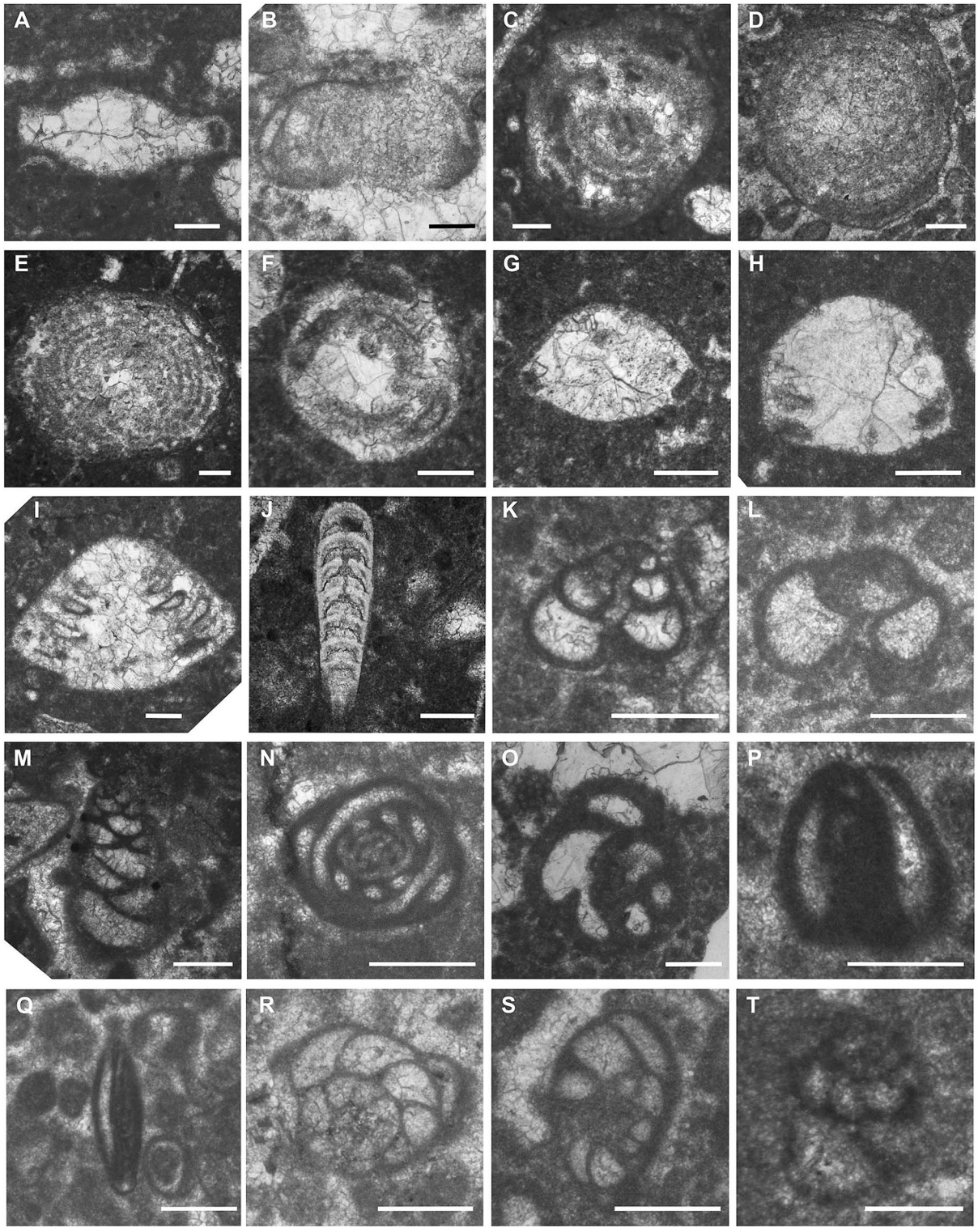

Fig. 5. Benthic foraminifera of the Valle Agricola section. A) *Aulotortus tumidus* (9.8 m); B) *Aulotortus impressus* (34.0 m); C) *Aulosina oberhauseri* (9.8 m); D) *Triasina hantkeni* (23 m); E) *Triasina hantkeni* (211.6 m); F) *Parvalamella friedli* (211.4 m); G) *Lamelliconus permodiscoides* (211.3 m); H) *Frentzenella crassa* (168.3 m); I) *Trocholina* sp. (14.7 m); J) *Austrocolomia* sp. (166.5 m); K) *"Trochammina" almtalensis* (40.7 m); L) *"Trochammina" alpina* (3.8 m); M) *Duotaxis metula* (119.9 m); N) *Gandinella falsofriedli* (13.3 m); O) *Endoteba* sp. (199.0 m); P) *Miliolipora* sp. (186.7 m); Q) Ophthalmidiidae (141.3 m); R) Duostominidae (16.8 m); S) Duostominidae (205.3 m); T) Duostominidae (211.6 m). Scale bar is 200 μm for photographs A-S, it is 100 μm for photograph T. Numbers in parentheses refer to height from the base of the section.

maximum of 0‰ at 94.5 m. The upper part of the section (156.8–245 m) is characterized by a rising trend, with $\delta^{18}O_{carb}$ values reaching a maximum of 0‰ at 229.7 m.

3.3. Mt. Sparagio

3.3.1. Lithofacies, fossil associations and bioevents

The quality of the rock exposure is rather poor. A few beds reveal a distinct peritidal cyclicity, with mud-dominated facies capped by microbial laminites and/or red paleosols (see also Todaro et al., 2017). In most beds, a thick patina of superficial alteration prevents the observation of depositional textures and sedimentary structures, which are revealed only by exposing fresh surfaces. Depositional lithofacies are often overprinted by a network of dissolution cavities with geopetal infills of internal sediment, crystal silt and cement. Despite these limitations, eight lithofacies are recognized at Mt. Sparagio (Table 3; File S1). The section is divided in two intervals, mainly based on the fossil content (Fig. 6).

Interval A (0–177.8 m) consists of peritidal cycles with fossiliferous base-of-cycle facies containing megalodontid bivalves with maximum shell size of 20 cm and benthic foraminifera. Dasycladacean algae are also abundant in some beds. Benthic foraminifera are mainly represented by involutinids. The most significant taxa are: *Aulotortus* spp. (Fig. 7A-B), *Triasina hantkeni* (Fig. 7C), *Parvalamella friedli* (Fig. 7D), *Lamelliconus permodiscoides* (Fig. 7E), *Frentzenella crassa* and *Trocholina* spp. (Fig. 7F-H). Lageninids, possibly falling in the range of variability of the genera *Polarisella* (Fig. 7I) and *Austrocolomia*, textulariinids assigned to the genera *Duotaxis*, *"Tetrataxis"* (Fig. 7J), and *"Trochammina"* (Fig. 7K) are represented by rare specimens. Very rare specimens of robertininids (family Duostominidae: Fig. 7L) are observed in two samples (at 167 and 168.2 m). Dasycladacean algae are mainly represented by *Griphoporella curvata* (Fig. 7M). The HO of *T. hantkeni* is identified at 164.9 m, followed by the HO of *Aulotortus, Parvalamella*, and *Lamelliconus*, and of *Griphoporella curvata* at 177.1 m. The uppermost bed with megalodontid bivalves marks the top of interval A, at 177.8 m.

Interval B (177.8–250.6 m) consists of peritidal cycles with very poor macrofossil associations represented by fragments of small bivalves and gastropods. Microfossil associations are characterized by *T. parvovesiculifera* (Fig. 7N), which is the only abundant taxon, and by rare *Aeolissaccus dunningtoni* (Fig. 7O), textulariinid benthic foraminifera (Fig. 7P) and ostracods.

3.3.2. Carbon and oxygen stable isotopes

The $\delta^{13}C_{carb}$ values range overall between −1.8 and +3.5‰ with most values between −1 and +2‰ (Fig. 6). The carbon isotope profile shows high-amplitude fluctuations of up to 4‰ over stratigraphic intervals <2 m thick, especially between 0 and 145 m. These short-term fluctuations are superimposed on a series of positive excursions that are tens of meters thick. The first positive excursion is observed between 0 and 41.7 m, with $\delta^{13}C_{carb}$ reaching a peak of +2.4‰ at 23 m. A second excursion is observed between 41.7 and 69 m, with a $\delta^{13}C_{carb}$ peak of +1.9‰ at 56.6 m. A third excursion is observed between 69 and 89.5 m, with a peak of +1.7‰ at 73.7 m. The fourth excursion is observed between 73.7 and 142.5 m, with a peak of +1.3‰ at 124.6 m. The largest-scale and broadest positive $\delta^{13}C_{carb}$ excursion occurs between 142.5 and 250 m, reaching a maximum value of +3.55‰ at 195.4 m. The rising limb of this excursion is notably characterized by lower-amplitude fluctuations compared to the rest of the section.

The $\delta^{18}O_{carb}$ values range overall between −4 and +2‰ with most values lying between −3 and −1‰ (Fig. 6). The oxygen isotope profile shows high-amplitude/short-term fluctuations of up to 3‰ over short stratigraphic intervals <3 m thick throughout the section. The most striking feature of the $\delta^{18}O_{carb}$ profile is a high-amplitude (+4‰) positive excursion starting at 187.2 m and ending at about 200 m, with the $\delta^{18}O_{carb}$ reaching a maximum value of +1.8‰ at 191 m. This positive excursion coincides with a dolomitized interval (see paragraph 4.5).

4. Discussion

4.1. Biozonation of the studied sections

Several biozonations were proposed for Upper Triassic–Lower Jurassic Tethyan carbonate platforms, mainly based on benthic foraminifera and dasycladacean algae (Gaździcki, 1983; Septfontaine, 1984; De Castro, 1991; Chiocchini et al., 1994; Barattolo and Romano, 2005; Mancinelli et al., 2005; BouDagher-Fadel and Bosence, 2007; Velić, 2007; Romano et al., 2008; BouDagher-Fadel, 2018). In this study, we apply a biozonation derived by the integration of the zonal schemes introduced by Gaździcki (1983) for the West Carpathians (Slovakia and Poland), and by Chiocchini et al. (1994) for the central Apennines (Italy) (Fig. 8). A similar scheme was adopted by Mancinelli et al. (2005) for the

Table 3
Lithofacies of the Mt. Sparagio section. Relative abundances given as number of specimens/abiotic grains per thin section as follows: vr (very rare) = 1; r (rare) = 2–3; f (frequent) = 4–10; c (common) 10–25; vc (very common) = 25–50; a (abundant) > 50.

Mt. Sparagio				
Lithofacies	Texture	Abiotic components	Fossil content	Depositional environment
Megalodontid floatstone (Fb)	Floatstone in mudstone-wackestone matrix	Peloids (f)	Bivalves (a), matrix: foraminifera (c) and dasycladaceans (c), ostracods (r), *T. parvovesiculifera* (vr), gastropods (r)	Subtidal lagoon
Peloidal and bioclastic mudstone-wackestone (MWpb)	Mudstone-wackestone	Peloids (r), intraclasts (r), oncoids (r)	Bivalve fragments (f), foraminifera (f) and dasycladaceans (r), gastropods (r), ostracods (r), echinoid spines (r), *T. parvovesiculifera* (r)	Subtidal lagoon
Homogeneous mudstone (M)	Mudstone	Intraclasts (r)	Foraminifera (r), dasycladaceans (vr), gastropods (r), ostracods (r), *T. parvovesiculifera* (vr)	Subtidal lagoon
Oncoidal floatstone-rudstone (FRo)	Floatstone-rudstone	Peloids (a), intraclasts (a)	Bivalve fragments (r), foraminifera (vr), gastropods (r), ostracods (r)	Subtidal lagoon
Peloidal-intraclastic-bioclastic packstone-grainstone (PGpib)	Packstone-grainstone	Peloids (a), intraclasts (a), oncoids (vr), ooids (vr)	Bivalve fragments (r), foraminifera (f) and dasycladaceans (r), echinoid spines (r), gastropods (vr), ostracods (r), *T. parvovesiculifera* (f-c)	Subtidal lagoon
Fenestral mudstone-wackestone (MWf)	Mudstone-wackestone	Peloids (r); intraclasts (vr), black pebbles (vr)	*T. parvovesiculifera* (f), foraminifera (r), ostracods (r)	Tidal flat (intertidal)
Microbial laminite (LAM)	Bindstone	Peloids (r), intraclasts (c)	Foraminifera (r), ostracods (r), *T. parvovesiculifera* (r)	Tidal flat (intertidal-supratidal)
Paleosol (PAL)	Mudstone	Intraclasts (c), lithoclasts (c)	Barren	Subaerial

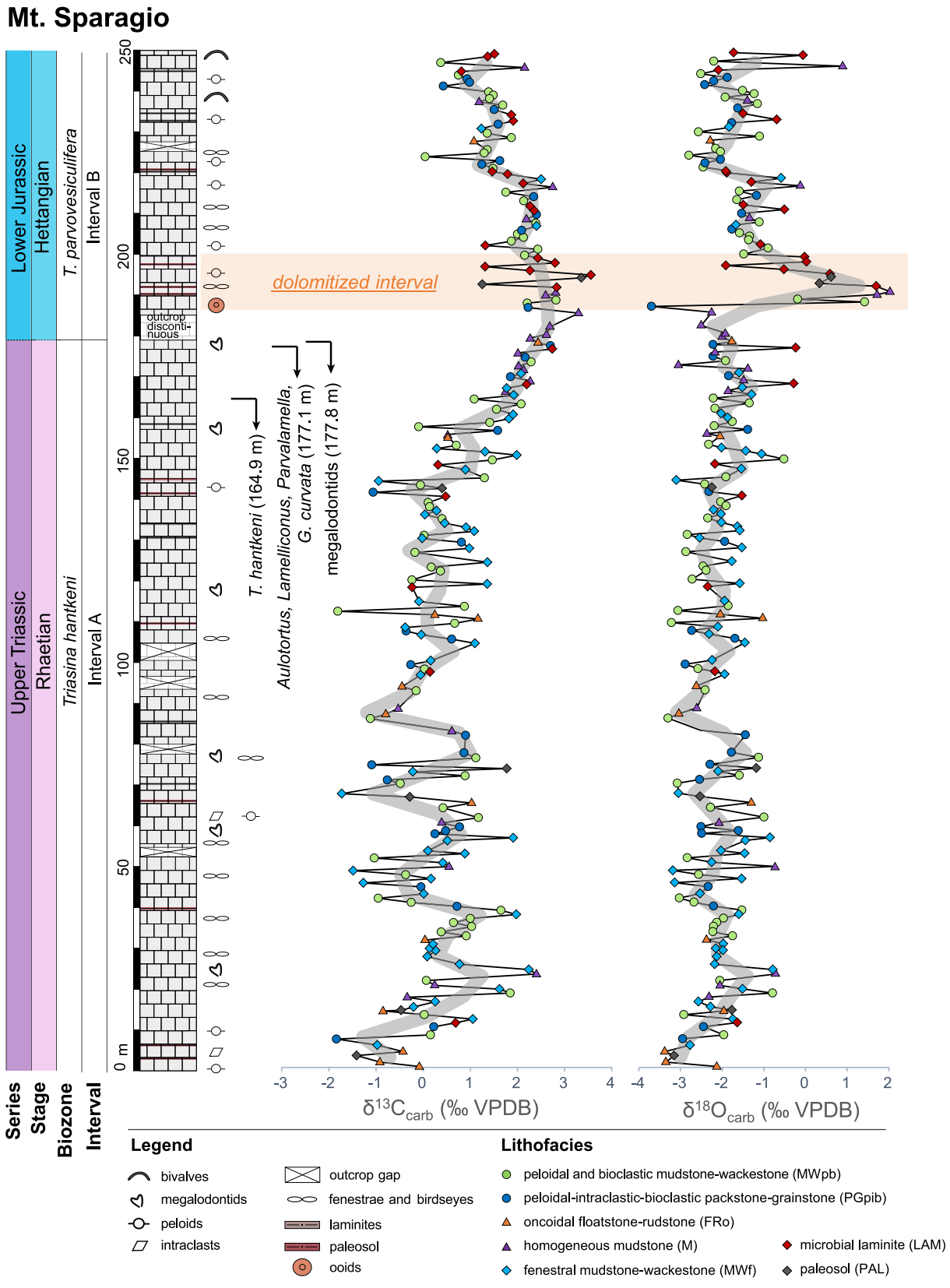

Fig. 6. Litho-, biostratigraphy and stable isotope profiles ($\delta^{13}C_{carb}$ and $\delta^{18}O_{carb}$) of the Mt. Sparagio section (Panormide Carbonate Platform, Sicily, Italy). Interval A is fossil-rich and its top is defined by the extinction of megalodontid bivalves. Interval B is poorly fossiliferous and dominated by *Thaumatoporella parvovesiculifera*. The Triassic/Jurassic boundary is approximated to the extinction level of megalodontid bivalves (see paragraph 4.2). The gray line in the stable isotope profiles represents a 5 m moving average. The dolomitized interval is discussed in paragraph 4.5.

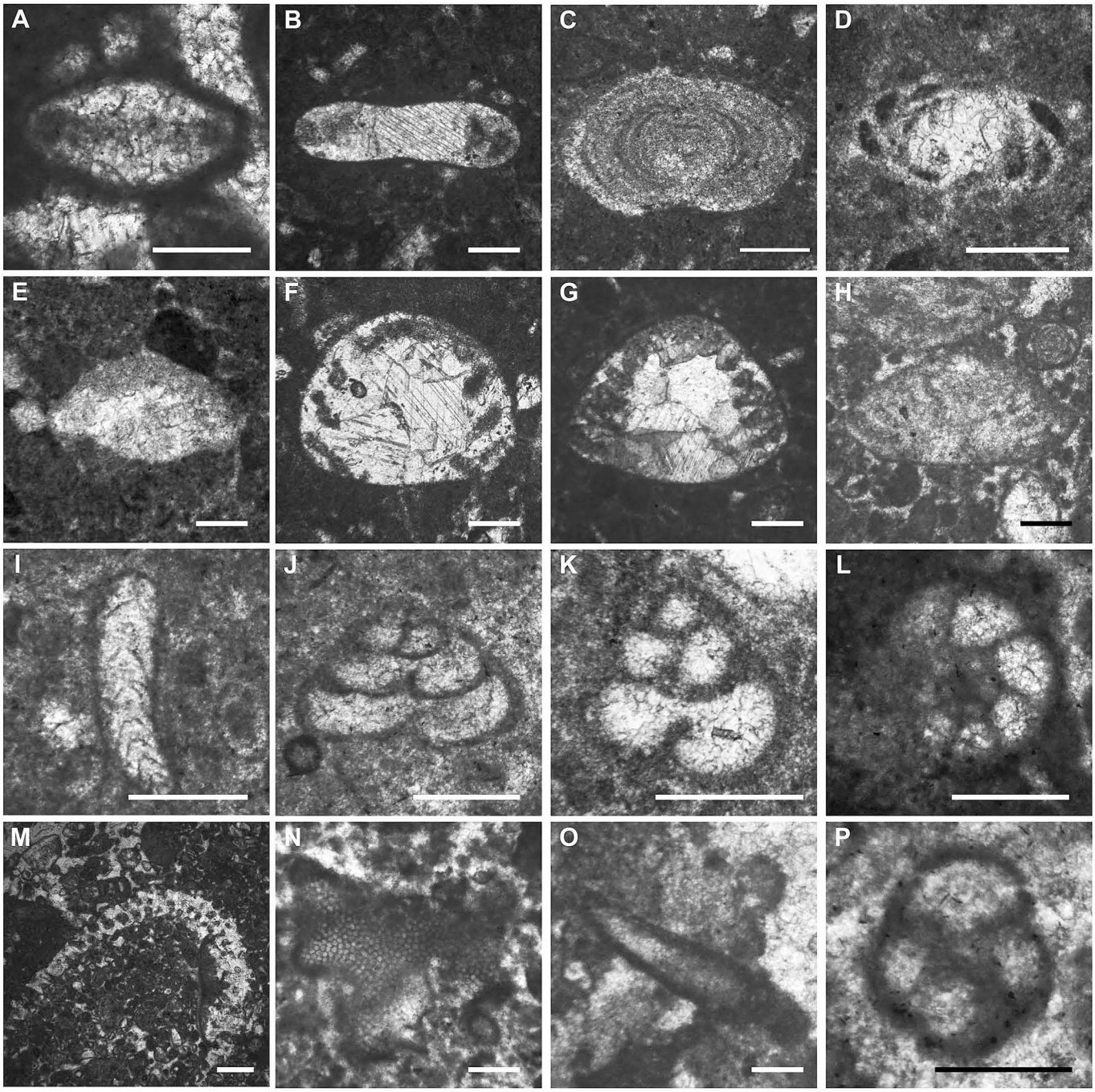

Fig. 7. Microfossils of the Mt. Sparagio section. A) *Aulotortus communis* (174.0 m); B) *Aulotortus impressus* (169.4 m); C) *Triasina hantkeni* (164.3 m); D) *Parvalamella friedli* (177.1 m); E) *Lamelliconus permodiscoides* (168.7 m); F) *Frentzenella crassa* (169.4 m); G) *Frentzenella crassa* or *Trocholina* sp. (173.1 m); H) ?*Trocholina* sp. (168.7 m); I) *Polarisella* sp. (164.9 m); J) *"Tetrataxis" inflata* (144.4 m); K) *"Trochammina"* cf. *alpina* (168.7 m); L) Duostominidae (167.0 m); M) *Griphoporella curvata* (169.4 m); N) *Thaumatoporella parvovesiculifera* (225.4 m); O) *Aeolisaccus dunningtoni* (198.6 m); P) "*Trochammina*" sp. (247.9 m). Scale bar is 200 μm for photographs A-B, D-L, N—P, it is 500 μm for photographs C, M. Numbers in parentheses refer to height from the base of the section.

Valle Agricola section and by Romano et al. (2008) for the Mt. Messapion section.

The lowermost biozone in our scheme is the *Aulosina oberhauseri* (=*Triasina oberhauseri* after Rigaud et al., 2012a) Zone following Gaździcki (1983) (Fig. 8). This biozone is present only in the lowermost portion (0–23 m) of interval A in the Valle Agricola section, below the LO of *T. hantkeni* (Fig. 4).

The overlying *Triasina hantkeni* Zone is defined by the LO and HO of *T. hantkeni* (Fig. 8). The dasycladacean alga *Griphoporella curvata* is commonly found in assemblages of this biozone (Chiocchini et al., 1994; Mancinelli et al., 2005; Romano et al., 2008), but it is also reported from older stratigraphic intervals (Barattolo et al., 1993), therefore it cannot be used as a marker for the *T. hantkeni* Zone. The remaining part of interval A at Valle Agricola (23–211.6 m) and the whole interval A at Mt. Messapion (0–52.7 m) are assigned to the *T. hantkeni* Zone, based on the occurrence of the marker species (Figs. 2 and 4). Interval A at Mt. Sparagio (0–177.8 m) is also assigned to the *T. hantkeni* Zone, based on the occurrence of the nominal species up to 164.9 m, of other involutinids up to 177.1 m (e.g., *Aulotortus*, *Lamelliconus*, and *Parvalamella* species) and of megalodontid bivalves up to 177.8 m (Fig. 6).

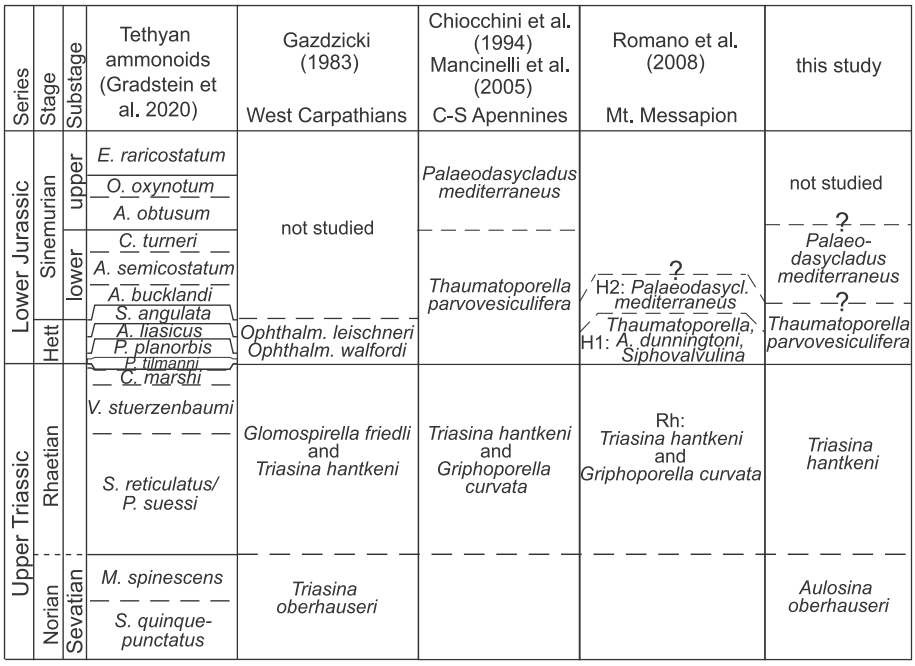

Fig. 8. Biozonations of Upper Triassic – Lower Jurassic carbonate platforms. Chronostratigraphy after Gradstein et al. (2020).

The overlying *Thaumatoporella parvovesiculifera* Zone corresponds to the interval between the HO of the *T. hantkeni* assemblage (i.e., *T. hantkeni*, *Aulotortus*, *Lamelliconus*, and *Parvalamella*) and of megalodontid bivalves, and the LO of *Palaeodasycladus mediterraneus* (Fig. 8). The *T. parvovesiculifera* Zone is recognized at Mt. Messapion (52.7–224.5 m) and corresponds to the whole interval B, where *T. parvovesiculifera* is the only common microfossil, and to the lower part of interval C (Fig. 2). Interval B of the Valle Agricola section (211.6–245 m) is also attributed to the *T. parvovesiculifera* Zone, considering that Mancinelli et al. (2005) reported the occurrence of this taxon in this section for ca 100 m between the HO of *T. hantkeni* and the LO of *P. mediterraneus* (Fig. 4). Interval B of the Mt. Sparagio section (177.8–250 m) is also entirely attributed to the *T. parvovesiculifera* Zone, and corresponds to the interval from the top of the *T. hantkeni* Zone to the top of the section (Fig. 6).

The overlying *Palaeodasycladus mediterraneus* Zone is defined at its base by the LO of the nominal taxon (Fig. 8). This biozone is recognized only in the uppermost part of interval C at Mt. Messapion (224.5–293 m), based on the LO of the *P. mediterraneus* at 224.5 m (Fig. 2).

4.2. Chronostratigraphic calibration of the bioevents defining the carbonate platform biozones

The LO of *T. hantkeni* is here used to approximate the Norian/Rhaetian boundary in agreement with Gaździcki (1983), because in sections containing conodonts this species has been consistently found at or slightly above the LO of *Misikella posthernsteini* (Slovakia, Poland and Hungary: Gaździcki et al., 1979, Gaździcki, 1983; Indonesia: Martini et al., 1997; Slovenia: Gale et al., 2012; Italy: Jadoul et al., 2012), which is the current candidate primary event to define the base of the Rhaetian Stage (Krystyn et al., 2007; Bertinelli et al., 2016; Ogg et al., 2020). An exception is observed in the paleoequatorial sections of the United Arab Emirates, where *T. hantkeni* has been reported below the LO of *M. posthernsteini* (Maurer et al., 2015; Davies and Simmons, 2018; Ge, 2021; Urban et al., 2023). The conodont-controlled late Norian age of *T. hantkeni* mentioned by Urban et al. (2023) for the Northern Calcareous Alps (NCA, Austria) and referred to the work of Reijmer and Everaars (1991) requires further studies, because the specimen illustrated in the latter paper as *T. hantkeni* likely falls in the range of variability of *A. oberhauseri*.

The HO of the *T. hantkeni* assemblage and of megalodontid bivalves is used to approximate the Rhaetian/Hettangian boundary, in agreement with previous biozonations of Triassic–Jurassic Tethyan carbonate platforms (e.g., Gaździcki, 1983; De Castro, 1991; Chiocchini et al., 1994; Mancinelli et al., 2005; Velić, 2007; Romano et al., 2008). This chronostratigraphic calibration is supported by the sequence of events observed in the carbonate platforms bordering the intraplatform basins of the NCA (Golebiowski and Braunstein, 1988; McRoberts et al., 1997; Mette et al., 2016), where the HO of *T. hantkeni*, *Aulotortus* species and megalodontid bivalves is broadly coeval to the extinction of Rhaetian ammonites and conodonts, and slightly precedes the first appearance of the ammonite *Psiloceras spelae tirolicum*, which defines the base of the Hettangian Stage at the GSSP section of Kuhjoch (Eiberg Basin, NCA, Austria: Hillebrandt, 2013).

The LO of *P. mediterraneus* has been regarded as a late Hettangian to late Sinemurian event (Sartoni and Crescenti, 1962; De Castro, 1987, 1991; Chiocchini et al., 1994; Barattolo and Romano, 2005; Mancinelli et al., 2005; Romano et al., 2008). However, all the sections in the southern Alps and northern Apennines where the LO of *P. mediterraneus* can be constrained by ammonoids, indicate an early Sinemurian age for this event, most probably falling in the Bucklandi (index species *Arietites bucklandi*) or Semicostatum (index species *Arnioceras semicostatum*) Chronozone (see supplementary material File S1 and Fig. S1.7 for further details).

4.3. Extinction patterns across the TJB interval

The TJB in the studied section is approximated to the extinction level of *T. hantkeni* and *G. curvata* at Mt. Messapion and Valle Agricola, and of megalodontid bivalves at Mt. Sparagio (Fig. 9), as discussed in paragraphs 4.1 and 4.2.

In the studied sections, the sequence of bioevents across the TJB displays similar patterns: Rhaetian involutinids disappear together with *G. curvata* at the top of the *T. hantkeni* Zone, and with Duostominidae at Mt. Messapion and Valle Agricola. The extinction level of Duostominidae cannot be precisely established at Mt. Sparagio as they occur in two samples only (at 167 and 168.2 m), likely for adverse ecological conditions. A highest occurrence close to the TJB for this group is also

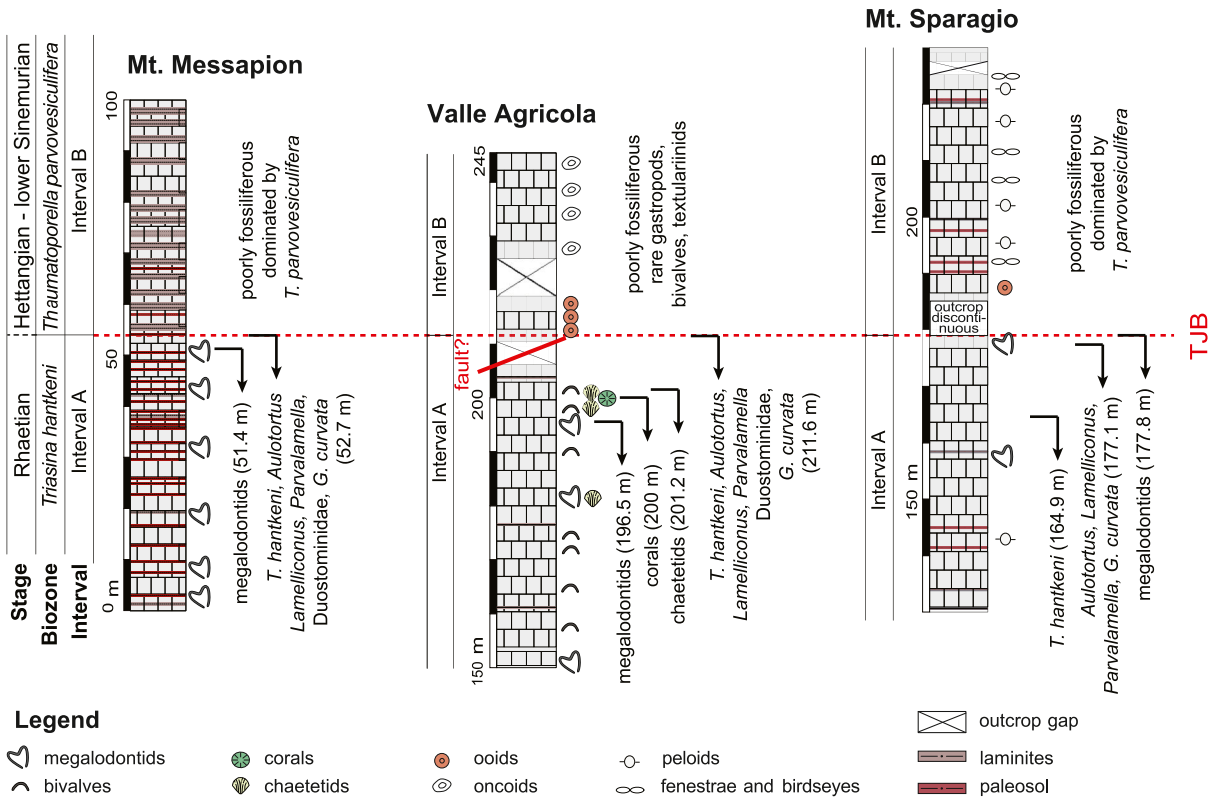

Fig. 9. Patterns of extinction of Rhaetian carbonate platform taxa in the three studied sections.

documented in the Mt. Cefalo (Latium, Italy, Southern Apennines: Mancinelli et al., 2005) and Slovenian (Gale et al., 2011) sections. *Triasina hantkeni* disappears together with the other involutinids at Mt. Messapion and Valle Agricola. The earlier disappearance of *T. hantkeni* in the Mt. Sparagio section, about 12 m below the HO of the other involutinids, might be due to its rare occurrence under locally unfavorable environmental conditions.

The HO of megalodontid bivalves is very close to the top of the *T. hantkeni* Zone at Mt. Messapion and Mt. Sparagio. At Valle Agricola, the HO of megalodontids is about 15 m below this level. This difference might be partly due to the poor exposure of the upper part of the Valle Agricola section, where a 4 m-thick interval below the last bed with Rhaetian fossils is covered by vegetation and a thick soil and could not be investigated (Fig. 9).

Summing up, the extinction of the typical Dachstein-type association, dominated by megalodontids, involutinid foraminifera and dasycladacean algae, coincides with the top of the *T. hantkeni* Zone in the studied sections. Poor exposure and local paleoenvironmental conditions are probably responsible for the slight differences in the extinction level of Rhaetian taxa in individual sections.

It is worth noting that the ETE severely affected carbonate platform assemblages from the backreef lagoon to the reef front. Dasycladacean algae (Barattolo and Romano, 2005; Bucur and Reolid, 2024), bivalves (Kiessling and Aberhan, 2007), corals (Kiessling et al., 2009; Martindale et al., 2012), and chaetetids (West, 2015) suffered high extinction rates. However, relatively few species among foraminifera became extinct during the ETE. The family Milioliporidae (miliolids), which preferentially lived close to the carbonate platform edge (Schäfer and Senowbari-Daryan, 1981; Zaninetti et al., 1992; Martini et al., 1997) and has a very sporadic occurrence in the studied sections, disappears at the TJB, as well as the Duostominidae (robertininids). Involutinids were severely affected by the ETE. Nevertheless, several genera (e.g., *Involutina* and *Trocholina*) that are absent in the studied sections above the TJB, survived the event in refugium areas (Rigaud et al., 2015; Gale et al., 2020) and diversified during the Early Jurassic (Rigaud et al., 2013). Textulariinids and lageninids, which were adapted to different habitats from the backreef lagoon to basinal deeper water settings, were nearly unaffected by the ETE, and show increased diversity during the Hettangian (Tappan and Loeblich, 1988; Kaminski et al., 2010).

4.4. Stratigraphic continuity and facies changes across the TJB

Deposition in shallow waters makes carbonate platform sections particularly susceptible to non-deposition and/or erosion during episodes of subaerial exposure. For this reason, we have examined in detail the intervals across the biostratigraphically defined TJB looking for sedimentological evidence of significant stratigraphic gaps.

At Mt. Messapion, the uppermost bed with Rhaetian benthic foraminifera and dasycladacean algae is a subtidal bioclastic packstone-grainstone, overlain by 40 cm of whitish dolomitized microbial laminite that is capped by a laterally discontinuous cm-thick red paleosol. This shallowing-upward peritidal cycle is similar to the other cycles occurring in interval A and in the lower part of interval B. The paleosol at its top documents an interval of subaerial exposure. The duration of the hiatus associated with the paleosol cannot be constrained by biostratigraphy as it coincides with the boundary between two adjacent biozones (see Fig. 9). Interval B shows the same peritidal cyclicity as interval A (see also Romano et al., 2008), but with subtidal facies characterized by very low diversity assemblages dominated by *T. parvovesiculifera*. In this section, in agreement with Romano et al. (2008), the level of the HO of Rhaetian fossils is considered to represent the true extinction of these taxa, as it does not coincide with a sharp facies change nor with evidence of a significant stratigraphic gap.

At Valle Agricola, the uppermost sample with Rhaetian foraminifera and dasycladacean algae is a bioclastic wackestone, which passes upward, within the same bed, into an ooid grainstone. The contact is a sharp surface that does not preserve any evidence of subaerial exposure and is therefore interpreted as a submarine erosional surface. The

presence of a minor stratigraphic gap associated with this surface cannot be excluded, but carbon-isotope correlation with other records excludes the presence of a major hiatus (see paragraph 4.6). Above the extinction level, the section continues with ~5 m of ooid packstone-grainstone. Low-diversity fossil assemblages, consisting of gastropods, rare bivalve shells and textulariinid benthic foraminifera, are documented in the overlying oncoid grainstone-rudstone.

At Mt. Sparagio, the uppermost bed with megalodontids is observed at 177.8 m. In the overlying 7 m-thick stratigraphic interval, the quality of the outcrop is discontinuous, due to a thick soil and vegetation cover.

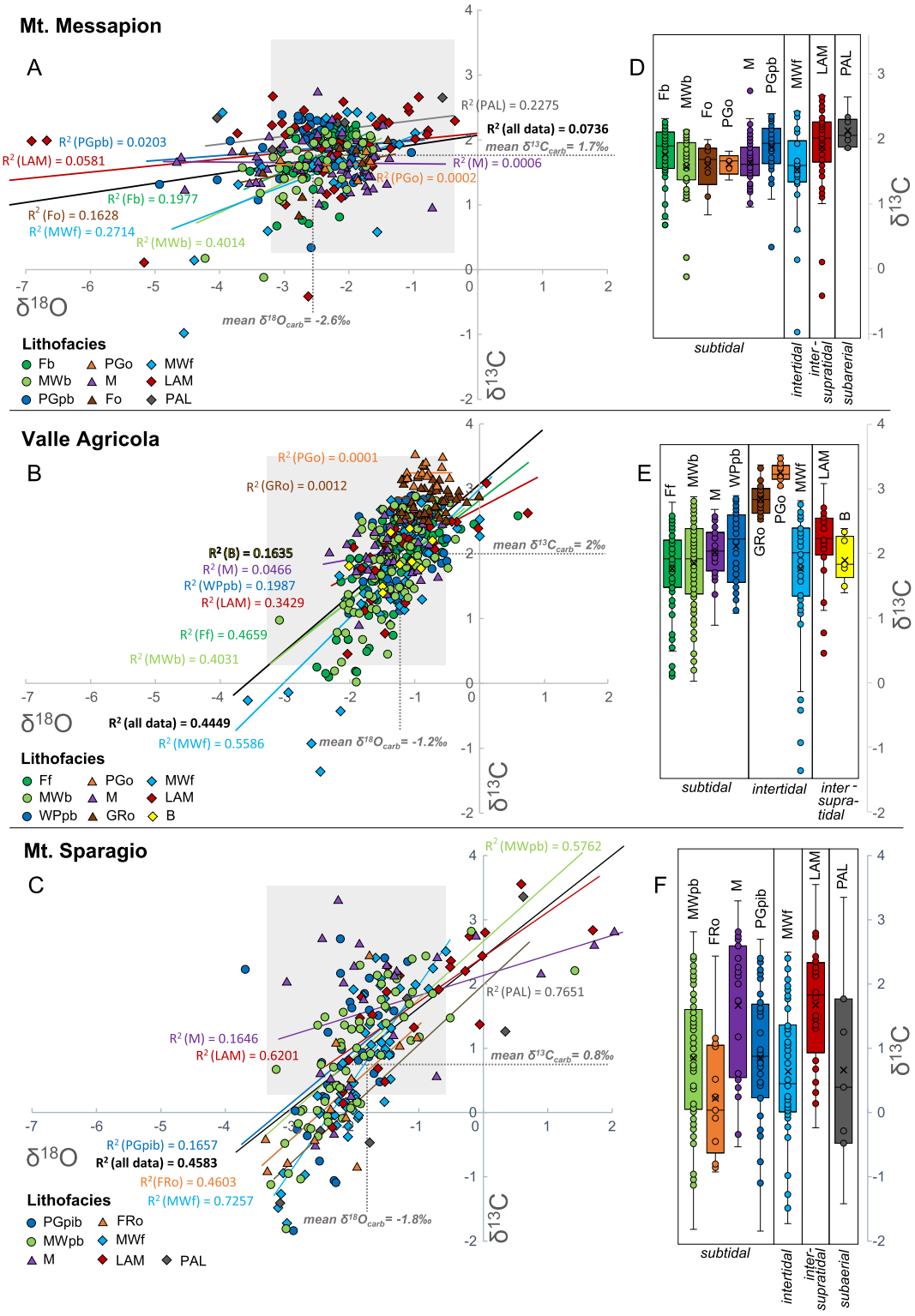

Fig. 10. $\delta^{13}C$ and $\delta^{18}O$ crossplots and $\delta^{13}C$ whisker plots of the studied sections. A) $\delta^{13}C_{carb}$ and $\delta^{18}O_{carb}$ crossplot of the Mt. Messapion section; B) $\delta^{13}C_{carb}$ and $\delta^{18}O_{carb}$ crossplot of the Valle Agricola section. C) $\delta^{13}C_{carb}$ and $\delta^{18}O_{carb}$ crossplot of the Mt. Sparagio section; D) $\delta^{13}C_{carb}$ whisker plots for the lithofacies of the Mt. Messapion section; E). $\delta^{13}C_{carb}$ whisker plots for the lithofacies of the Valle Agricola section; F) $\delta^{13}C_{carb}$ whisker plots for the lithofacies of the Mt. Sparagio section. The gray area shows the range of oxygen and carbon stable isotope values exhibited by Norian-Rhaetian low latitude brachiopod shells after Prokoph et al. (2008).

The few beds exposed in this interval consist of peloidal-intraclastic mudstone-wackestone with rare *T. parvovesiculifera*. Above this interval, the section continues with peritidal cycles capped by microbial laminites and fenestral mudstones. The subtidal facies show very low-diversity assemblages dominated by *T. parvovesiculifera*. As at Mt. Messapion, the HO of Rhaetian fossils does not coincide with a facies change nor with evidence of a significant stratigraphic gap, therefore it is considered to represent the true extinction of these taxa, in agreement with Todaro et al. (2017, 2018, 2022).

4.5. Reliability of the $\delta^{13}C_{carb}$ record in the studied sections

Carbon-isotope stratigraphy represents a crucial technique for accurately dating and correlating stratigraphic sections. However, the reliability of carbon isotope data must be carefully evaluated because several factors can cause deviations of the local carbon isotope trend from the global signal. These include biological fractionation, local paleoceanographic conditions (Weber and Woodhead, 1969; Patterson and Walter, 1994) and post-depositional diagenetic alteration (e.g., Dickson and Coleman, 1980). In particular, deposition in shallow-waters frequently exposes carbon platform sediments to meteoric diagenesis, potentially imparting depleted $\delta^{13}C_{carb}$ values to levels below subaerial exposure surfaces, reflecting the influence of soil-derived CO_2 (Allan and Matthews, 1982; Lohmann, 1988; Joachimski, 1994; Immenhauser et al., 2008). Moreover, shallow-water limestones consist of a wide textural and mineralogical variety of skeletal and non-skeletal components, whose relative abundance might influence the isotopic signal recorded by bulk samples.

Assessing the influence of local environmental conditions and of diagenesis is of paramount importance before attempting any stratigraphic correlation based on the carbon-isotope record. Strong covariation between $\delta^{13}C_{carb}$ and $\delta^{18}O_{carb}$ is commonly taken as evidence of diagenetic alteration due to meteoric water influx in the mixing zone (Allan and Matthews, 1982), or of a trend of decreasing alteration within the freshwater phreatic zone (Swart, 2011). Therefore, we tested the reliability of the carbon isotope records of the three studied sections by evaluating the covariation of carbon- and oxygen-isotope data (Fig. 10A-C). Correlation coefficients between $\delta^{13}C_{carb}$ and $\delta^{18}O_{carb}$ values were also calculated separately for each lithofacies, in order to highlight whether the stable isotope signal is influenced by the depositional and early diagenetic conditions. The relationship between lithofacies and the $\delta^{13}C_{carb}$ signal is further investigated through the whisker plots (Fig. 10D-F).

The correlation coefficients between the carbon- and oxygen isotope values calculated for each section (all data) are very low for Mt. Messapion ($R^2 = 0.07$; Fig. 10A), moderate for Valle Agricola ($R^2 = 0.44$; Fig. 10B) and Mt. Sparagio ($R^2 = 0.46$; Fig. 10C), suggesting an overall minor to moderate diagenetic overprint (e.g., Immenhauser et al., 2008; Huck et al., 2017). The subaerial to intertidal lithofacies (PAL, LAM, MWf) generally yield among the highest R^2 of each section and a higher variability in the $\delta^{13}C_{carb}$ and $\delta^{18}O_{carb}$ values, with several outliers in the whisker plots (Fig. 10D-F). This is in line with the expectations that these top-of-cycle lithofacies are more exposed to the effects of meteoric diagenesis.

The data-points of each lithofacies do not plot as separate clusters in the cross-plots of $\delta^{13}C_{carb}$ vs $\delta^{18}O_{carb}$ (Fig. 10A-C), suggesting that the isotopic signal is not significantly influenced by the lithofacies type. Further support to this observation is provided by the whisker plots, showing that almost all lithofacies have interquartile $\delta^{13}C_{carb}$ ranges broadly overlapping, except for the ooid packstone-grainstone and oncoid grainstone-rudstone of Valle Agricola (Fig. 10E). Ooid precipitation is mediated by diverse autotroph/heterotroph microbial communities, which may deviate the isotopic signal far from the equilibrium of the ambient seawater and shift the $\delta^{13}C_{carb}$ toward more positive values via enhanced photosynthetic activity (Diaz et al., 2015; Chen et al., 2022). However, it is worth noting that the positive $\delta^{13}C_{carb}$ excursion encompassing the extinction of Rhaetian taxa in the Valle Agricola section is not controlled by the occurrence of ooid grainstones as it starts a few meters below and continues across the facies change (Fig. 4).

Most of the samples of the studied sections have stable isotope values falling within the range of Late Triassic (Norian-Rhaetian) seawater (Fig. 10A-C) reconstructed from low latitude brachiopod shells (Prokoph et al., 2008). The Mt. Messapion section shows some samples with very negative $\delta^{18}O_{carb}$ and invariant $\delta^{13}C_{carb}$ values, likely reflecting a moderate influence of late burial diagenesis (Marshall, 1992; Immenhauser et al., 2003, 2008). The Mt. Sparagio section displays some samples with enriched $\delta^{18}O_{carb}$ values obtained in the dolomitized interval between 188.5 and 198.4 m (Fig. 10C, F). The $\delta^{18}O_{carb}$ of these samples is about 2–3‰ more positive compared to the samples of adjacent levels, which is roughly the expected difference between calcite and dolomite precipitated at equilibrium from the same fluid (Vasconcelos et al., 2005). In all sections, some samples are shifted toward more negative $\delta^{13}C_{carb}$ and $\delta^{18}O_{carb}$ values with respect to the Late Triassic seawater (Fig. 10A-C), a trajectory that suggests early meteoric diagenesis (Allan and Matthews, 1982; Joachimski, 1994; Immenhauser et al., 2008). In the Mt. Messapion and Valle Agricola section such depleted values are mainly recorded in supra- to intertidal (LAM, MWf) lithofacies, whereas at Mt. Sparagio they are also recorded in subtidal lithofacies (FRo, PGpib, MWpb), suggesting a more pervasive influence of meteoric diagenesis in the latter section.

Summing up, minor to moderate diagenetic alteration, mostly due to meteoric diagenesis, certainly affected the carbon-isotope ratios of some samples. The effects of diagenetic alteration are more severe at Mt. Sparagio, which displays the most negative and variable $\delta^{13}C_{carb}$ values (Fig. 10F) and the highest $\delta^{13}C_{carb}$ vs. $\delta^{18}O_{carb}$ correlation coefficients in almost all lithofacies (Fig. 10C). In all sections, meteoric diagenesis is likely responsible for some high-amplitude fluctuations toward negative $\delta^{13}C_{carb}$ values defined by one or few data-points recorded in supra- to intertidal lithofacies. However, the stable isotope values obtained during this study mostly fall within the range of Late Triassic tropical seawater. Moreover, crossplots and whisker plots (Fig. 10) show that the measured isotopic values are not controlled by the lithofacies type. These arguments support the hypothesis that at least the long-term trends and excursions of the $\delta^{13}C_{carb}$ profiles represent a faithful record of changes in the carbon isotope ratio of the global ocean, and as such could be used for global correlation.

A very important result of our study consists in the identification of the extinction level of Rhaetian assemblages within the upper part of a positive $\delta^{13}C_{carb}$ excursion that is consistently recorded in three carbonate platform sections that were located at a distance of hundreds of km and that underwent a different geologic evolution. This positive excursion is defined in each section by many data-points along stratigraphic intervals that are tens of meters thick, it persists across different lithofacies (i.e., it is not controlled by facies changes) and represents a +1 (Mt. Messapion) to +2.5‰ (Valle Agricola) deviation from pre- and post-excursion mean values. The amplitude of these excursions is comparable to other medium to large-scale isotopic events identified in Southern Tethyan carbonate platforms that have been linked to perturbations of the global carbon cycle (e.g., Trecalli et al., 2012; Frijia et al., 2015; Amodio and Weissert, 2017). All these observations, and the consistent occurrence at a correlative stratigraphic level in the three sections (see next paragraph), strengthen the hypothesis that the positive $\delta^{13}C_{carb}$ excursion encompassing the extinction level of Rhaetian fossil assemblages is a primary feature of the isotopic record of the global ocean.

4.6. Correlation of Tethyan carbonate platform sections and the timing of the extinction of the Dachstein-type biota

In the reference sections for the TJB interval (e.g., the GSSP section for the base of the Hettangian Stage at Kuhjoch, NCA, Austria, and St.

Audrie's Bay, proto-North Atlantic, SW Britain), the ETE has been linked to a series of negative isotopic excursions in the organic carbon record, which are known as the precursor, initial, and main CIE (e.g., Hesselbo et al., 2002; Ruhl and Kürschner, 2011; Korte et al., 2018; Zaffani et al., 2018). In particular, the initial CIE is broadly coeval to the onset of the CAMP emplacement and to the extinction of many fossil groups (e.g., ammonoids) (Hesselbo et al., 2002; Whiteside et al., 2010; Ruhl and Kürschner, 2011; Kent et al., 2017; Lindström et al., 2017; Korte et al., 2018; Ruhl et al., 2020; Wignall and Atkinson, 2020). The data presented in the previous paragraphs show that the HO of Rhaetian carbonate platform assemblages falls within the rising limb of a $\delta^{13}C_{carb}$ positive excursion in the Pelagonian, Apennine, and Panormide carbonate platforms. Correlating the $\delta^{13}C_{carb}$ profiles of these carbonate platform sections with the $\delta^{13}C_{org}$ profiles of the reference TJB sections is complicated by the absence of ammonoids and conodonts in shallow-water sections and by the apparent decoupling of the $\delta^{13}C_{carb}$ and $\delta^{13}C_{org}$ records across the TJB (e.g., Clémence et al., 2010a, 2010b; Bachan et al., 2012; Bartolini et al., 2012; Ge, 2021).

For this reason, we attempted a correlation based on the bio- and carbon-isotope stratigraphy for all the Southern Tethyan carbonate platform sections for which a well-resolved $\delta^{13}C_{carb}$ record is available. Subsequently, we compared the timing and patterns of extinction in Southern Tethyan carbonate platforms with those documented in the classical sections of the Lombardy Basin and NCA, for which the $\delta^{13}C_{carb}$ is also available (Fig. 11).

A bio-chemostratigraphic pattern very similar to that documented in the studied sections is observed at equatorial paleolatitudes in the Ghalilah Fm of the United Arab Emirates, where the extinction of Rhaetian assemblages (the coral *Retiophyllia*, bivalves and brachiopods) occurs at the top of the Sumra Mb, within a positive $\delta^{13}C_{carb}$ excursion, a few meters below the onset of a $\delta^{13}C_{carb}$ decreasing trend (Maurer et al., 2008; Al-Suwaidi et al., 2016; Ge et al., 2018) (Fig. 11). The HO of Rhaetian carbonate platform assemblages falls a few meters below the peak of the $\delta^{13}C_{carb}$ positive excursion, and therefore appears to be broadly synchronous with the extinction documented in the three carbonate platforms studied. By contrast, the extinction of *T. hantkeni* and megalodontid bivalves in the Mt. Cefalo section (southern Apennines, Latium, Italy) falls below a 2 m-thick caliche horizon where a major short-lived $\delta^{13}C_{carb}$ negative excursion is recorded (Mancinelli et al., 2005; Bachan et al., 2012) (Fig. 11). Previous studies suggested that the geochemical signal might be affected by meteoric alteration and that the stratigraphic record is probably incomplete (Bachan et al., 2012).

In the classical sections of the Lombardy Basin, the HO of *T. hantkeni* and megalodontid bivalves occurs at the boundary between the shallow-water carbonate succession of the Calcare di Zu Fm and the poorly fossiliferous marls of the Malanotte Fm, slightly below a short-lived negative $\delta^{13}C_{carb}$ excursion that has been correlated with the initial CIE (Galli et al., 2005, 2007; Bachan et al., 2012; Bottini et al., 2016; option 1 in Zaffani et al., 2018). At Lorüns, the disappearance of in-situ Rhaetian assemblages of the backreef lagoon coincides with the switch to the carbonate-poor lithologies of the Schattwald beds and occurs slightly below a major short-lived negative excursion that has been correlated with the initial CIE (McRoberts et al., 1997; Felber et al., 2015). In other Dachstein-type sections (e.g., Steinernes Meer, NCA, Austria; Tata, Transdanubian Range, Hungary), previous studies documented a significant stratigraphic gap across the TJB, between Rhaetian fossil-rich backreef lagoon and reef carbonates and the overlying Hettangian to Sinemurian poorly fossiliferous limestones (Krystyn et al., 2005; Felber et al., 2015; Pálfy et al., 2021).

In addition, the $\delta^{13}C_{carb}$ record of Southern Tethyan carbonate platforms shows a single positive excursion across the TJB interval, while in the Val Adrara section (Lombardy Basin) two positive excursions were documented (P1 and P2 of Bachan et al., 2012). The P1 excursion falls at the base of the Malanotte Fm, and according to palynomorph (HO of *Rhaetipollis germanicus*: Galli et al., 2005, 2007) and calcareous nannofossil (HO of *Prinsiosphaera triassica* and LO of *Schizosphaerella punctulata*: Bottini et al., 2016) bioevents, and to organic carbon-isotope stratigraphy (Zaffani et al., 2018) lies very close to the TJB. The P2 excursion falls about 50 m above the LO of *S. punctulata* (Bottini et al., 2016) and well within the Hettangian Albenza Fm, which documents the recovery of the carbonate platform after the TJB carbonate crisis (Jadoul and Galli, 2008).

Bachan et al. (2012) suggested that the P1 excursion at Mt. Cefalo is elided by a hiatus at the level of the caliche horizon and that the only positive excursion of this section correlates with P2 at the base of the Albenza Fm. However, our data indicate that the $\delta^{13}C_{carb}$ positive excursion encompassing the extinction of Rhaetian taxa in four Southern Tethyan carbonate platform sections (except for Mt. Cefalo) cannot correspond to the rising limb of P2 in the Lombardy Basin, because P2 falls well within the Hettangian (Jadoul and Galli, 2008; Bachan et al., 2012; Bottini et al., 2016). Instead, we suggest that this positive excursion is correlatable with the P1 positive peak recorded in the Malanotte Fm (Fig. 11). According to this correlation, the extinction of Rhaetian assemblages in the resilient carbonate platforms at the tropical and equatorial paleolatitudes of Southern Tethys slightly postdates that documented in the classical sections of the NCA and Lombardy Basin (Fig. 11). The resilient Southern Tethyan carbonate platforms document, therefore, the true extinction level of the Dachstein-type biota, while the sections at the northern margin of the Tethys Ocean might represent a pseudoextinction due to the demise of the carbonate platform. Notably, this pattern of carbonate platform demise at higher latitudes and more resilient carbonate platforms at lower latitudes was documented during other global paleoenvironmental perturbations like the early Aptian oceanic anoxic event (Weissert et al., 1998; Skelton and Gili, 2012).

4.7. Patterns and timing of recovery after the ETE in Southern Tethyan carbonate platforms

The ETE in Southern Tethyan carbonate platforms is characterized by the sharp and synchronous disappearance of highly fossiliferous Rhaetian associations. These assemblages are substituted by low-diversity associations dominated by *T. parvovesiculifera* in sections where peritidal facies persisted above the ETE (Mt. Messapion, Mt. Sparagio), and by cyanophycean nodules and small gastropods in sections where peritidal facies are sharply overlain by ooid-oncoid grainstone-rudstone (Valle Agricola). This low-diversity interval ("survival interval" of Barattolo and Romano, 2005) is tens of meters thick and, with reference to carbon isotope stratigraphy, extends from the upper part of the rising limb to the end of the $\delta^{13}C_{carb}$ P1 excursion (Fig. 11). This interval testifies a shift in the dominant carbonate production style, from prolific aragonitic biomineralization (megalodontid bivalves, involutinid benthic foraminifera, dasycladacean algae), to $CaCO_3$ precipitation mediated by microbial activity (microbial laminites, ooids) or by relatively simple, small-sized organisms that dominate low diversity assemblages in the aftermath of ecologic crisis (e.g., *T. parvovesiculifera*) and are here interpreted as "r-strategists", in agreement with Barattolo and Romano (2005) and Romano et al. (2008).

The recovery of carbonate platform ecosystems after the ETE was very slow. The progressive re-appearance and diversification of textulariinid benthic foraminifera in carbonate platform assemblages occurred in the Hettangian. The dasycladalean algae regained their role as dominant carbonate producers several Myr after the ETE, seemingly in the early Sinemurian, with the appearance of *P. mediterraneus*, accompanied in some localities by *Tersella* and *Fanesella* spp. (Barattolo and Romano, 2005; Mancinelli et al., 2005). The return of larger benthic foraminifera was even more delayed, with rich and diverse assemblages appearing in the late Sinemurian-Pliensbachian (Septfontaine, 1984).

Very similar patterns are observed in other Southern Tethyan carbonate platform sections across the TJB (Ghalilah Fm, United Arabian Emirates: Maurer et al., 2008; Al-Suwaidi et al., 2016; Ge et al., 2018; Urban et al., 2023; Tahtaiskele section, western Turkey: Coskun

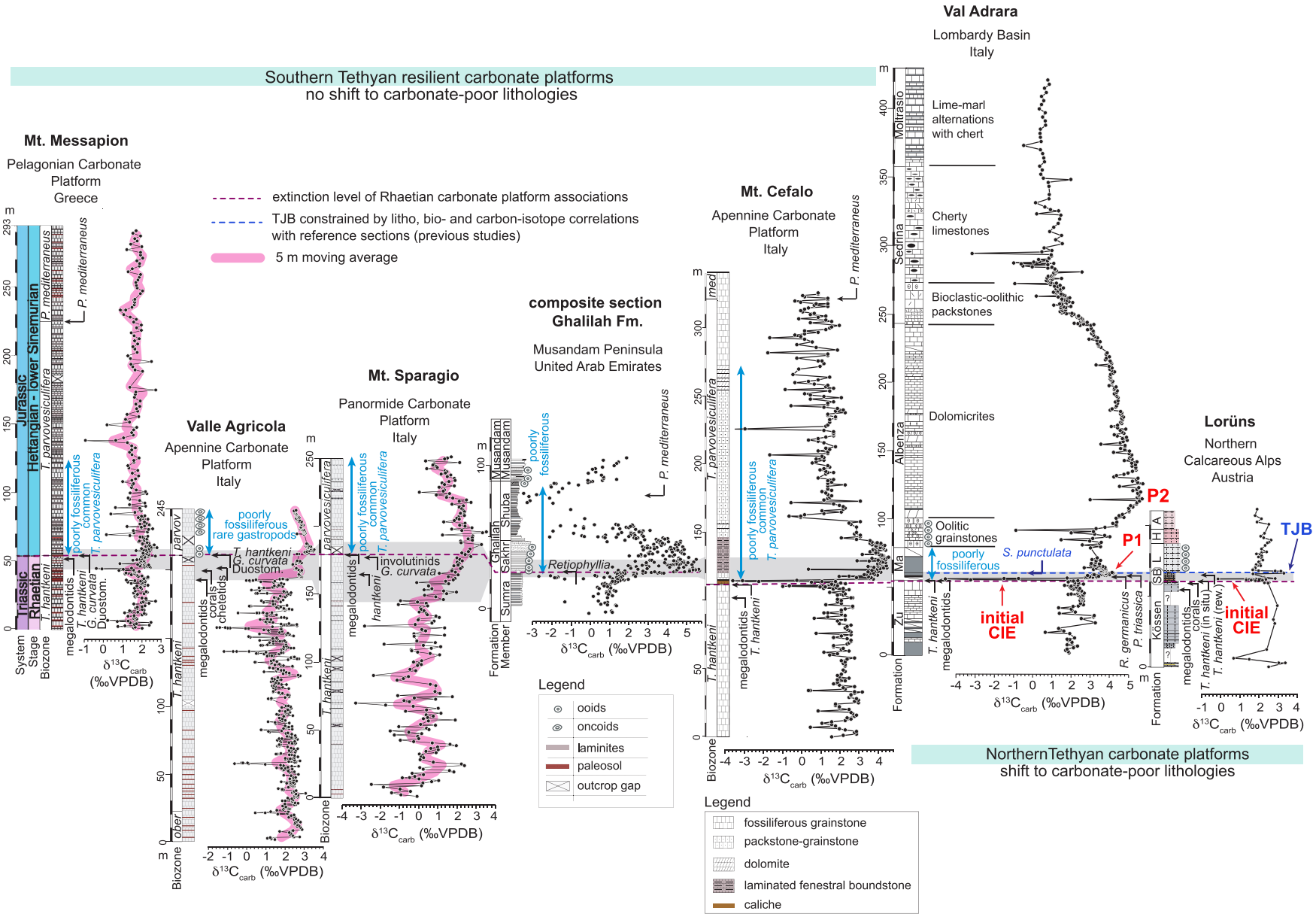

Fig. 11. The litho-, bio- and carbon-isotope record of Tethyan carbonate platforms across the TJB interval: Mt. Messapion, Valle Agricola and Mt. Sparagio after this study; litho- and biostratigraphy of the composite section of the Ghalilah Fm after Maurer et al. (2008), Al-Suwaidi et al. (2016), Hönig et al. (2017), and Urban et al. (2023), carbon-isotope record after Ge et al. (2018), the stratigraphic log refers to the Wadi Naqab section of Hönig et al. (2017); Mt. Cefalo after Mancinelli et al. (2005) and Bachan et al. (2012); lithostratigraphy and carbon-isotope record of Val Adrara after Bachan et al. (2012); biostratigraphy after Galli et al. (2005, 2007) and Bottini et al. (2016); Lorüns after Felber et al. (2015). Position of the TJB at Val Adrara and Lorüns according to Bottini et al. (2016) and Felber et al. (2015), respectively. The positive carbon-isotope peaks P1 and P2 are after Bachan et al. (2012). The gray band indicates a likely correlative stratigraphic interval defined at the base by the onset of a $\delta^{13}C_{carb}$ increasing trend and at the top by the onset of a decreasing trend. The dashed purple line highlights the diachronous extinction level of Rhaetian carbonate platform associations in the Tethys Ocean, as it falls within the gray band in Southern Tethyan resilient carbonate platforms (except for the incomplete Mt. Cefalo section) and below the gray band in Northern Tethyan carbonate platforms (see text for further details). All sections are illustrated with the same vertical scale. Abbreviations: Duostom. = Duostominidae; *ober.* = *Aulosina oberhauseri*; *parvov.* = *T. parvovesiculifera*; *med* = *P. mediterraneus*; Sakhr = Sahkra; Ma = Malanotte; SB=Schattwald beds; L = Lorüns; H=Hierlatz; A = Adnet. (For interpretation of the references to colour in this figure legend, the reader is referred to the web version of this article).

Tunaboylu et al., 2014) and therefore emerge as general evolutionary patterns of low-latitude shallow-water ecosystems.

5. Conclusions

In this paper we document the facies, and the bio- and carbon-isotope stratigraphy of three Southern Tethyan carbonate platform sections across the Late Triassic–Early Jurassic time interval: Mt. Messapion (Greece), Valle Agricola, and Mt. Sparagio (Italy). These sections are particularly relevant for investigating the tempo and mode of ecosystem response to the ETE, because they witness persistent shallow-water carbonate sedimentation across the TJB interval.

In the studied sections, the ETE is documented by the disappearance of rich and diverse Rhaetian associations dominated by megalodontid bivalves, involutinid foraminifera and dasycladacean algae within the rising limb of a positive $\delta^{13}C_{carb}$ excursion. A similar pattern is observed in the Ghalilah Fm of the United Arab Emirates, representative of a carbonate platform at subequatorial paleolatitude. The reproducibility of this bio- and chemostratigraphic pattern in different paleogeographic domains suggests that it is not biased by diagenetic alteration or by local paleoceanographic conditions. We suggest that the positive $\delta^{13}C_{carb}$ excursion encompassing the extinction of Rhaetian taxa in Southern Tethyan carbonate platforms is correlative with the positive $\delta^{13}C_{carb}$ excursion documented above the initial negative CIE in the lowermost part of the Malanotte Fm in the Lombardy Basin and in the Schattwald beds at Lorüns (NCA). According to this correlation, the extinction of Rhaetian carbonate platform assemblages in the Southern Tethyan domain represents the true extinction level of the Dachstein-type biota, whereas its disappearance at the initial CIE in the NCA and Lombardy Basin likely represents a pseudoextinction caused by the demise of the carbonate platform.

The extinction level of Rhaetian taxa is overlain by an interval characterized by low-diversity fossil assemblages dominated by *T. parvovesiculifera* at Mt. Messapion and Mt. Sparagio, where peritidal facies persisted above the TJB, and by small gastropods and cyanophycean nodules at Valle Agricola, where peritidal facies are sharply overlain by ooid-oncoid grainstone-rudstones. The low-diversity post-extinction interval testifies for a shift of the dominant carbonate producers, from aragonitic biocalcifiers (megalodontid bivalves, involutinid benthic foraminifera, dasycladacean algae) to calcitic r-strategists (e.g., *T. parvovesiculifera*) and microbial carbonate precipitation (microbial laminites, ooids).

For the first time, our study highlights a paleogeographic and/or latitudinal pattern in the response of benthic biocalcifiers and of carbonate platform ecosystems to the environmental perturbations at the TJB interval. At higher latitudes, on the northern margin of the Tethys Ocean, the Dachstein-type biota and the carbonate platform ecosystems failed to adapt to the environmental perturbations associated with the initial CIE. Rhaetian assemblages in Southern Tethys were instead resilient and survived this crisis, but subsequent and/or persistent environmental stress ultimately caused their extinction globally. Despite the extinction of the most prolific aragonitic biocalcifiers, tropical and equatorial carbonate platforms of Southern Tethys kept growing through a change in the dominant style of carbonate production and a shift to chemical or microbially-mediated $CaCO_3$ precipitation. The ecosystem recovery was slow and gradual, and healthy carbonate platforms with rich and diverse assemblages of biocalcifiers (dasycladacean algae) re-appeared in Southern Tethys some Mys after the ETE, in the early Sinemurian.

CRediT authorship contribution statement

Andrea Montanaro: Writing – original draft, Investigation, Formal analysis, Data curation, Conceptualization. **Francesca Falzoni:** Writing – original draft, Investigation, Formal analysis, Data curation, Conceptualization. **Alessandro Iannace:** Writing – original draft, Funding acquisition, Formal analysis. **Mariano Parente:** Writing – original draft, Investigation, Funding acquisition, Formal analysis.

Declaration of competing interest

The authors declare that they have no known competing financial interests or personal relationships that could have appeared to influence the work reported in this paper.

Data availability

The authors confirm that the data supporting the findings of this study are available within the article and its supplementary materials.

Acknowledgments

We gratefully acknowledge the editor Lucia Angiolini, the guest editor of the special issue “Biocalcifier resilience and response during global climate changes” and the anonymous reviewers for their comments and suggestions that greatly improved the quality of this manuscript.

This paper is a contribution to the research project PRIN2017 RX9XXXY, funded by the Italian Ministero dell’Istruzione, dell’Università e della Ricerca. AM gratefully acknowledges the financial support by SEPM (Student Assistance Grant), AAPG (Grant in Aid) and IAS (Postgraduate Research Grant). We would like to express our appreciation to Nicolas Carras (IGME, Greece) for assisting with the fieldwork authorization for the Mt. Messapion section. Giovanna Della Porta and Elena Ferrari (University of Milan, Italy), Gianluca Frijia and Valentina Brombin (University of Ferrara, Italy) are acknowledged for their assistance and acquisition of stable isotope data. Roberto Rettori (University of Perugia, Italy) is warmly thanked for his advice on the identification of foraminifera.

Appendix A. Taxonomic appendix

The taxonomic identification of benthic foraminiferal taxa is based on the species and genus concepts given in the original descriptions and illustrations and takes into account Loeblich and Tappan (1988), and the revisions by Piller (1978) and Rigaud et al. (2012a, 2012b, 2013) for involutinids, and Gale et al. (2018) for the genus *Siphovalvulina*. Identification of representatives of the families Duostominidae Brotzen (1963), Milioliporidae Brönnimann and Zaninetti (1971), and Ophthalmiididae Wiesner (1920) follows their original description and Loeblich and Tappan (1988). Discrimination between *Duotaxis*, “*Tetrataxis*” and *Siphovalvulina* follows Haig et al. (2021). The genus “*Tetrataxis*” is quoted and regarded as textulariinid because Mesozoic specimens show a finely agglutinated single-layered wall that differs from the calcareous double-layered wall exhibited by the Paleozoic representatives of this genus (Loeblich and Tappan, 1988). “*Trochammina*” is quoted because Triassic species assigned to this genus have an agglutinated likely calcitic-cemented wall, whereas the wall of the type-species (i.e., the modern species *Trochammina inflata* Montagu, 1808) is finely agglutinated, imperforate and organic-cemented, and thus Triassic “*Trochammina*” should be moved to a different genus (Haig et al., 2007). The undetermined textulariinids, mentioned in the text and figures, include specimens that cannot be determined at the genus level, because of poor preservation or non-diagnostic cuts. They also include taxa that have not been described in the literature yet, and whose description will be the purpose of future works.

Taxonomic list of species and genera, with author(s) and year of description identified during this study and mentioned in the text and/or figures, listed in alphabetical order.

Foraminifera:

Genus *Aulosina* Rigaud, Martini, and Rettori, 2013

Aulosina oberhauseri (Koehn-Zaninetti and Brönnimann, 1968)
Genus *Aulotortus* Weynschenk, 1956
Aulotortus communis (Kristan, 1957)
Aulotortus impressus (Kristan-Tollmann, 1964)
Aulotortus sinuosus Weynschenk, 1956
Aulotortus tumidus (Kristan-Tollmann, 1964)
Genus *Austrocolomia* Oberhauser, 1960
Genus *Duotaxis* Kristan, 1957
Duotaxis birmanica Zaninetti and Brönnimann, 1975
Duotaxis metula Kristan, 1957
Genus *Endoteba* Vachard and Razgallah, 1988
Genus *Endotriadella* Vachard, Martini, Rettori, and Zaninetti, 1994
Genus *Everticyclammina* Redmond, 1964
Genus *Frentzenella* Rigaud et al., 2013
Frentzenella crassa (Kristan, 1957)
Genus *Gandinella* Ciarapica and Zaninetti, 1985
Gandinella falsofriedli (Salaj, Borza and Samuel, 1983)
Genus *Glomospira* Rzehak, 1885
Genus *Involutina* Terquem, 1962
Genus *Lamelliconus* Piller, 1978 emend. Rigaud et al., 2013
Lamelliconus permodiscoides (Oberhauser, 1964)
Genus *Miliolipora* Brönnimann and Zaninetti, 1971
Genus *Parvalamella* Rigaud, Martini and Rettori, 2012
Parvalamella friedli (Kristan-Tollmann, 1962)
Genus *Polarisella* Mamet and Pinard, 1992
Genus *Radoicicina* Gale et al., 2018
Radoicicina ciarapicae Gale et al., 2018
Genus *Siphovalvulina* Septfontaine, 1988 emend. Gale et al., 2018
Siphovalvulina cf. *colomi* BouDagher-Fadel, Rose, Bosence and Lord, 2001
"Tetrataxis" inflata Kristan, 1957
Genus *Triasina* Majzon, 1954
Triasina hantkeni Majzon, 1954
"Trochammina" almtalensis Koehn-Zaninetti, 1969
"Trochammina" alpina Kristan-Tollmann, 1964
Genus *Trocholina* Paalzow, 1922 emend. Rigaud et al., 2013
Dasycladacean algae:
Genus *Griphoporella* Pia, 1915
Griphoporella curvata (Gümbel, 1872) Pia, 1915
Genus *Palaeodasycladus* Pia, 1927
Palaeodasycladus mediterraneus (Pia, 1920)
Incertae sedis:
Genus *Aeolissaccus* Elliot, 1958
Aeolissaccus dunningtoni Elliot, 1958
Genus *Thaumatoporella* Pia, 1927
Thaumatoporella parvovesiculifera (Raineri, 1922)

Taxonomic list of species and genera with author(s) and year of description mentioned in the text and identified by previous studies, listed in alphabetical order.

Ammonoids:
Arietites bucklandi Sowerby, 1818
Arnioceras semicostatum Young and Bird, 1829
Psiloceras spelae Guex et al., 1998 subsp. *tirolicum* Hillebrandt and Krystyn, 2009
Calcareous nannofossils:
Prinsiosphaera triassica Jafar, 1983
Schizosphaerella punctulata Deflandre and Dangeard, 1938
Conodonts:
Misikella posthernsteini Kozur and Mock, 1974
Corals:
Retiophyllia Culf, 1967
Dasycladacean algae:
Fanesella Cros and Lemoine, 1967
Tersella Morellet, 1951
Palynomorphs:
Rhaetipollis germanicus Schulz, 1967

Appendix B. Supplementary data

Supplementary data to this article can be found online at https://doi.org/10.1016/j.palaeo.2024.112335.

References

Allan, J.R., Matthews, R.K., 1982. Isotope signatures associated with early meteoric diagenesis. Sedimentology 29, 797–817.
Al-Suwaidi, A.H., Steuber, T., Suarez, M.B., 2016. The Triassic–Jurassic boundary event from an equatorial carbonate platform (Ghalilah Formation, United Arab Emirates). J. Geol. Soc. Lond. 173, 949–953.
Amodio, S., Weissert, H., 2017. Palaeoenvironment and palaeoecology before and at the onset of Oceanic Anoxic Event (OAE) 1a: Reconstructions from Central Tethyan archives. Palaeogeogr. Palaeoclimatol. Palaeoecol. 479, 71–89.
Bachan, A., van de Schootbrugge, B., Fiebig, J., McRoberts, C.A., Ciarapica, G., Payne, J. L., 2012. Carbon cycle dynamics following the end-Triassic mass extinction: Constraints from paired $\delta^{13}C_{carb}$ and $\delta^{13}C_{org}$ records. Geochem. Geophys. Geosyst. 13, Q09008.
Barattolo, F., Romano, R., 2005. Shallow carbonate platform bioevents during the Upper Triassic-lower Jurassic; an evolutive interpretation. Boll. Soc. Geol. Ital. 124, 123–142.
Barattolo, F., De Castro, P., Parente, M., 1993. Some remarks on *Griphoporella curvata* (Gümbel 1872) Pia 1915, dasycladacean green alga from the Upper Triassic. Studies on Fossil Benthic Algae. Bollettino della Società Paleontologica Italiana, Special 1, 23–45.
Bartolini, A., Guex, J., Spangenberg, J.E., Schoene, B., Taylor, D.G., Schaltegger, U., Atudorei, V., 2012. Disentangling the Hettangian carbon isotope record: Implications for the aftermath of the end-Triassic mass extinction. Geochem. Geophys. Geosyst. 13, Q01007.
Bernecker, M., 2005. Late Triassic reefs from the Northwest and South Tethys: distribution, setting, and biotic composition. Facies 51 (1), 442–453.
Bernoulli, D., 2001. Mesozoic-Tertiary carbonate platforms, slopes and basins of the external Apennines and Sicily. In: Vai, G.B., Martini, I.P. (Eds.), Anatomy of an Orogen: The Apennines and Adjacent Mediterranean Basins. Springer, Dordrecht, pp. 307–325.
Bertinelli, A., Casacci, M., Concheri, G., Gattolin, G., Godfrey, L., Katz, M.E., Maron, M., Mazza, M., Mietto, P., Muttoni, G., Rigo, M., Sprovieri, M., Stellin, F., Zaffani, M., 2016. The Norian/Rhaetian boundary interval at Pignola-Abriola section (Southern Apennines, Italy) as a GSSP candidate for the Rhaetian Stage: an update. Albertiana 43, 5–18.
Blackburn, T.J., Olsen, P.E., Bowring, S.A., McLean, N.M., Kent, D.V., Puffer, J., McHone, G., Rasbury, E.T., Et-Touhami, M., 2013. Zircon U-Pb geochronology links the end-Triassic extinction with the Central Atlantic Magmatic Province. Science 340, 941–945.
Bond, D.P.G., Wignall, P.B., 2014. Large igneous provinces and mass extinctions: an update. Spec. Pa. Geol. Soci. Am. 505, 29–55.
Bosellini, A., 2004. The western passive margin of Adria and its carbonate platforms. In: Crescenti, V., D'Offizi, S., Merlino, S., Sacchi, L. (Eds.), Geology of Italy. Special Volume of the Italian Geological Society for the IGC32, Florence, pp. 79–92.
Bottini, C., Jadoul, F., Rigo, M., Zaffani, M., Artoni, C., Erba, E., 2016. Calcareous nannofossils at the Triassic/Jurassic boundary: stratigraphic and paleoceanographic characterization. Riv. Ital. Paleontol. Stratigr. 122, 141–164.
BouDagher-Fadel, M.K., 2018. Evolution and Geological Significance of Larger Benthic Foraminifera. UCL press, London, p. 693.
BouDagher-Fadel, M.K., Bosence, D.W., 2007. Early Jurassic benthic foraminiferal diversification and biozones in shallow-marine carbonates of western Tethys. Senckenb. Lethaea 87, 1–39.
Bucur, I.I., Reolid, M., 2024. Incidence of the early Toarcian global change on Dasycladales (Chlorophyta) and the subsequent recovery: Comparison with end-Triassic Mass Extinction. Earth Sci. Rev. 249, 104666.
Celet, P., Clement, B., Ferrière, J., 1988. Evolution geodynamique de la plate-forme Pelagonienne au Mesozoic. Δελτίον της Ελληνικής Γεωλογικής Εταιρίας 20 (1), 215–222.
Chen, M., Conroy, J.L., Geyman, E.C., Sanford, R.A., Chee-Sanford, J.C., Connor, L.M., 2022. Stable carbon isotope values of syndepositional carbonate spherules and micrite record spatial and temporal changes in photosynthesis intensity. Geobiology 20, 667–689.
Chiocchini, M., Farinacci, A., Mancinelli, A., Molinari, V., Potetti, M., 1994. Biostratigrafia a foraminiferi, dasicladali e calpionelle delle successioni carbonatiche mesozoiche dell'Appennino centrale (Italia). Studi Geologici Camerti, Volume Speciale "Biostratigrafia dell'Italia centrale" 9–45.
Clémence, M.E., Bartolini, A., Gardin, S., Paris, G., Beaumont, V., Page, K.N., 2010a. Early Hettangian benthic–planktonic coupling at Doniford (SW England): Palaeoenvironmental implications for the aftermath of the end-Triassic crisis. Palaeogeogr. Palaeoclimatol. Palaeoecol. 295, 102–115.
Clémence, M.E., Gardin, S., Bartolini, A., Paris, G., Beaumont, V., Guex, J., 2010b. Bentho-planktonic evidence from the Austrian Alps for a decline in sea-surface carbonate production at the end of the Triassic. Swiss J. Geosci. 103, 293–315.
Coskun Tunaboylu, B., Altiner, D., Isintek, I., Demirci, D., 2014. Foraminiferal biostratigraphy and sequence stratigraphy of peritidal carbonates at the

Triassic–Jurassic boundary (Karaburun Peninsula, Western Turkey). J. Asian Earth Sci. 90, 61–76.
Dal Corso, J., Marzoli, A., Tateo, F., Jenkyns, H.C., Bertrand, H., Youbi, N., Mahmoudi, A., Font, E., Buratti, N., Cirilli, S., 2014. The dawn of CAMP volcanism and its bearing on the end-Triassic carbon cycle disruption. J. Geol. Soc. Lond. 171, 153–164.
D'Argenio, B., Alvarez, W., 1980. Stratigraphic evidence for crustal thickness changes on the southern Tethyan margin during the Alpine cycle. Geol. Soc. Am. Bull. 91, 681–689.
Davies, R.B., Simmons, M.D., 2018. Triassic sequence stratigraphy of the Arabian Plate. In: Pöppelreiter, M. (Ed.), Lower Triassic to Middle Jurassic Sequence of the Arabian Plate. Houten, The Netherlands, pp. 101–162.
De Castro, P., 1987. Le facies di piattaforma carbonatica del Giurassico italiano: diffusione areale e lineamenti biostratigrafici. Boll. Soc. Paleontol. Ital. 26, 309–325.
De Castro, P., 1991. Mesozoic. In: Barattolo, F., De Castro, P., Parente, M. (Eds.), 5th International Symposium on Fossil Algae. Field Trip Guide-Book, pp. 21–38. Giannini, Napoli.
Deenen, M.H., Ruhl, M., Bonis, N.R., Krijgsman, W., Kürschner, W.M., Reitsma, M., Van Bergen, M.J., 2010. A new chronology for the end-Triassic mass extinction. Earth Planet. Sci. Lett. 291, 113–125.
Dercourt, J., Gaetani, M., Vrielynck, B., Barrier, E., Biju-Duval, B., Brunet, M.F., Cadet, J. P., Crasquin, S., Sandulescu, M., 2000. Atlas Peri-Tethys, Palaeogeographical Maps. 24 Maps and Explanatory Notes. CCGM/CGMW, Paris, pp. 1–269.
Diaz, M.R., Swart, P.K., Eberli, G.P., Oehlert, A.M., Devlin, Q., Saeid, A., Altabet, M.A., 2015. Geochemical evidence of microbial activity within ooids. Sedimentology 62, 2090–2112.
Dickson, J.A.D., Coleman, M.L., 1980. Changes in carbon and oxygen isotope composition during limestone diagenesis. Sedimentology 27, 107–118.
Eltom, H.A., González, L.A., Hasiotis, S.T., Walker, D.J., Andrew, J.E., 2021. Calibration of bulk carbonate strontium isotopes to ammonite zones: Implication for global stratigraphic correlation of Callovian–Kimmeridgian strata in Central Saudi Arabia. Palaeogeogr. Palaeoclimatol. Palaeoecol. 564, 110083.
Felber, R., Weissert, H.J., Furrer, H., Bontognali, T.R.R., 2015. The Triassic–Jurassic boundary in the shallow-water marine carbonates from the western Northern Calcareous Alps (Austria). Swiss J. Geosci. 108, 213–224.
Flügel, E., 1981. Paleoecology and facies of Upper Triassic reefs in the northern Calcareous Alps: European fossil reef modelsSoc. Econ. Paleontol. Min. Spec. Publ. 30, 291–359.
Flügel, E., Senowbari-Daryan, B., 2001. Triassic reefs of the Tethys. In: Stanley, G.D. (Ed.), The History and Sedimentology of Ancient Reef Systems. Springer, Boston, MA, pp. 217–249.
Franceschi, M., Dal Corso, J., Posenato, R., Roghi, G., Masetti, D., Jenkyns, H.C., 2014. Early Pliensbachian (early Jurassic) C-isotope perturbation and the diffusion of the Lithiotis Fauna: Insights from the western Tethys. Palaeogeogr. Palaeoclimatol. Palaeoecol. 410, 255–263.
Frijia, G., Parente, M., Di Lucia, M., Mutti, M., 2015. Carbon and strontium isotope stratigraphy of the Upper cretaceous (Cenomanian-Campanian) shallow-water carbonates of southern Italy: Chronostratigraphic calibration of larger foraminifera biostratigraphy. Cretac. Res. 53, 110–139.
Gale, L., Rettori, R., Martini, R., Šmuc, A., Kolar-Jurkovšek, T., Rožič, B., 2011. Duostominidae (Foraminiferea, Robertinida) from the Upper Triassic beds of the Slovenian Basin (Southern Alps, Slovenia). Riv. Ital. Paleontol. Stratigr. 117, 375–397.
Gale, L., Kolar-Jurkovšek, T., Šmuc, A., Rožič, B., 2012. Integrated Rhaetian foraminiferal and conodont biostratigraphy from the Slovenian Basin, eastern Southern Alps. Swiss J. Geosci. 105, 435–462.
Gale, L., Barattolo, F., Rettori, R., 2018. Morphometric approach to determination of lower Jurassic siphovalvulinid foraminifera. Riv. Ital. Paleontol. Stratigr. 124, 265–282.
Gale, L., Rigaud, S., Gennari, V., Blau, J., Rettori, R., Martini, R., Gaetani, M., 2020. Recognition of upper Triassic temperate foraminiferal assemblages: Insights from the Khodz Group (NW Caucasus, Russia). Glob. Planet. Chang. 188, 103152.
Galli, M.T., Jadoul, F., Bernasconi, S.M., Weissert, H., 2005. Anomalies in global carbon cycling and extinction at the Triassic/Jurassic boundary: evidence from a marine C-isotope record. Palaeogeogr. Palaeoclimatol. Palaeoecol. 216, 203–214.
Galli, M.T., Jadoul, F., Bernasconi, S.M., Cirilli, S., Weissert, H., 2007. Stratigraphy and palaeoenvironmental analysis of the Triassic–Jurassic transition in the western Southern Alps (Northern Italy). Palaeogeogr. Palaeoclimatol. Palaeoecol. 244, 52–70.
Gaździcki, A., 1983. Foraminifers and biostratigraphy of Upper Triassic and lower Jurassic of the Slovakian and Polish Carpathians. Palaeontol. Pol. 44, 109–169.
Gaździcki, A., Kozur, H., Mock, R., 1979. The Norian-Rhaetian boundary in the light of micropaleontological data. Geologija 22 (1), 71–112.
Ge, Y., 2021. Decoupled $\delta^{13}C_{carb}$ and $\delta^{13}C_{org}$ records at Triassic–Jurassic boundary interval in eastern Tethys: Environmental implications for spatially different global response. Geosci. Front. 12, 101146.
Ge, Y., Shi, M., Steuber, T., Al-Suwaidi, A.H., Suarez, M.B., 2018. Environmental change during the Triassic–Jurassic boundary interval of an equatorial carbonate platform: Sedimentology and chemostratigraphy of the Ghalilah Formation, United Arab Emirates. Palaeogeogr. Palaeoclimatol. Palaeoecol. 502, 86–103.
Golebiowski, R., Braunstein, R.E., 1988. A Triassic/Jurassic boundary section in the Northern Calcareous Alps (Austria). IGCP Project 199, "rare events in Geology". Berichte der Geologischen Bundesanstalt 15, 39–46.
Gradstein, F.M., Ogg, J.G., Schmitz, M.D., Ogg, G.M., 2020. Geologic Time Scale 2020. Elsevier, Amsterdam.
Greene, S.E., Martindale, R.C., Ritterbush, K.A., Bottjer, D.J., Corsetti, F.A., Berelson, W. M., 2012. Recognising Ocean acidification in deep time: an evaluation of the evidence for acidification across the Triassic-Jurassic boundary. Earth Sci. Rev. 113, 72–93.
Haas, J., Pomoni-Papaioannou, F., Kostopoulou, V., 2009. Comparison of the late Triassic carbonate platform evolution and Lofer cyclicity in the Transdanubian Range, Hungary and Pelagonian Zone, Greece. Central Eur. Geol. 52 (2), 153–184.
Haig, D.W., McCartain, E., Barber, L., Backhouse, J., 2007. Triassic-lower Jurassic foraminiferal indices for Bahaman-type carbonate-bank limestones, Cablac Mountain, East Timor. J. Foraminifer. Res. 37, 248–264.
Haig, D.W., Rigaud, S., McCartain, E., Nano, J., Barros, I.S., Martini, R., 2021. Biostratigraphic indices for lower Jurassic carbonate-platform deposits (Perdido Group), Overthrust Terrane Association, Timor-Leste. J. Asian Ear. Sci. 215, 104797.
Hallam, A., 2002. How catastrophic was the end-Triassic mass extinction? Lethaia 35, 147–157.
Hallam, A., Wignall, P.B., 1997. Mass Extinctions and their Aftermath. Oxford University Press, UK, p. 328.
Hautmann, M., 2004. Effect of end-Triassic CO_2 maximum on carbonate sedimentation and marine mass extinction. Facies 50, 257–261.
Hesselbo, S.P., Robinson, S.A., Surlyk, F., Piasecki, S., 2002. Terrestrial and marine extinction at the Triassic-Jurassic boundary synchronized with major carbon-cycle perturbation: a link to initiation of massive volcanism? Geology 30 (3), 251–254.
Hillebrandt, A., Krystyn, L., Kürschner, W.M., Bonis, N.R., Ruhl, M., Richoz, S., Schobben, M.A., Urlichs, M., Bown, P.R., Kment, K., McRoberts, C.A., Simms, M., Tomäsových, A., 2013. The Global Stratotype Sections and Point (GSSP) for the base of the Jurassic System at Kuhjoch (Karwendel Mountains, Northern Calcareous Alps, Tyrol, Austria). Episodes 36, 162–198.
Hönig, M.R., John, C.M., Manning, C., 2017. Development of an equatorial carbonate platform across the Triassic-Jurassic boundary and links to global palaeoenvironmental changes (Musandam Peninsula, UAE, Oman). Gondwana Res. 45, 100–117.
Hönisch, B., Ridgwell, A., Schmidt, D.N., Thomas, E., Gibbs, S.J., Sluijs, A., Zeebe, R., Kump, L., Martindale, R.C., Greene, S.E., Kiessling, W., Ries, J., Zachos, J.C., Royer, D.L., Barker, S., Marchitto, T.M., Moyer, R., Pelejero, C., Ziveri, P., Foster, G. L., Williams, B., 2012. The Geological record of ocean acidification. Science 335, 1058–1063.
Huck, S., Wohlwend, S., Coimbra, R., Christ, N., Weissert, H., 2017. Disentangling shallow-water bulk carbonate carbon isotope archives with evidence for multi-stage diagenesis: an in-depth component-specific petrographic and geochemical study from Oman (mid-cretaceous). Depositional Rec. 3 (2), 233–257.
Immenhauser, A., Della Porta, G., Kenter, J.A.M., Bahamonde, J.R., 2003. An alternative model for positive shifts in shallow-marine carbonate $\delta^{13}C$ and $\delta^{18}O$. Sedimentology 50, 953–959.
Immenhauser, A., Holmden, C., Patterson, W.P., 2008. Interpreting the carbon-isotope record of ancient shallow epeiric seas: lessons from the recent. Dynam. Epeiric Seas 48, 137–174.
Jadoul, F., Galli, M.T., 2008. The Hettangian shallow water carbonates after the Triassic/Jurassic biocalcification crisis: the Albenza Formation in the Western Southern Alps. Riv. Ital. Paleontol. Stratigr. 114, 453–470.
Jadoul, F., Galli, M.T., Muttoni, G., Rigo, M., Cirilli, S., 2012. The late Norian-Hettangian stratigraphic and paleogeographic evolution of the Bergamasc Alps. Geoitalia, VI meeting FIST – Rimini, 2007. Geol. Field Trips 1–55.
Joachimski, M.M., 1994. Subaerial exposure and deposition of shallowing upward sequences: evidence from stable isotopes of Purbeckian peritidal carbonates (basal cretaceous), Swiss and French Jura Mountains. Sedimentology 41, 805–824.
Kaminski, M.A., Setoyama, E., Cetean, C.G., 2010. The Phanerozoic diversity of agglutinated foraminifera: origination and extinction rates. Acta Palaeontol. Pol. 55, 529–539.
Kent, D.V., Olsen, P.E., Muttoni, G., 2017. Astrochronostratigraphic polarity time scale (APTS) for the late Triassic and early Jurassic from continental sediments and correlation with standard marine stages. Earth Sci. Rev. 166, 153–180.
Kiessling, W., Aberhan, M., 2007. Geographical distribution and extinction risk: lessons from Triassic–Jurassic marine benthic organisms. J. Biogeogr. 34, 1473–1489.
Kiessling, W., Simpson, C., 2011. On the potential for ocean acidification to be a general cause of ancient reef crises. Glob. Chang. Biol. 17, 56–67.
Kiessling, W., Roniewicz, E., Villier, L., Léonide, P., Struck, U., 2009. An early Hettangian coral reef in southern France: Implications for the end-Triassic reef crisis. Palaios 24, 657–671.
Koglin, N., Kostopoulos, D., Reischmann, T., 2009. Geochemistry, petrogenesis and tectonic setting of the Samothraki mafic suite, NE Greece: Trace-element, isotopic and zircon age constraints. Tectonophysics 473, 53–68.
Korte, C., Ruhl, M., Pálfy, J., Ullmann, C.V., Hesselbo, S.P., 2018. Chemostratigraphy across the Triassic–Jurassic boundary. In: Sial, A.N., Gaucher, C., Ramkumar, M., Ferreira, V.P. (Eds.), Chemostratigraphy across Major Chronological Boundaries, American Geophysical Union, Geophysical Monograph, vol. 240, pp. 183–210.
Krystyn, L., Böhm, F., Kürschner, W.M., Delecat, S., Pálfy, J., Ozsvárt, P., 2005. The Triassic–Jurassic boundary in the Northern Calcareous Alps. In: Program, abstracts and field guide, 5th field workshop of IGCP 458 pp. A1-A14.
Krystyn, L., Richoz, S., Gallet, Y., Bouquerel, H., Kürschner, W.M., Spötl, C., 2007. Updated bio- and magnetostratigraphy from Steinbergkogel (Austria), candidate GSSP for the base of the Rhaetian Stage. Albertiana 36, 164–173.
Lindström, S., van De Schootbrugge, B., Hansen, K.H., Pedersen, G.K., Alsen, P., Thibault, N., Dybkjær, K., Bjerrum, C.J., Nielsen, L.H., 2017. A new correlation of Triassic–Jurassic boundary successions in NW Europe, Nevada and Peru, and the Central Atlantic Magmatic Province: a time-line for the end-Triassic mass extinction. Palaeogeogr. Palaeoclimatol. Palaeoecol. 478, 80–102.

Loeblich Jr., A.R., Tappan, H., 1988. Foraminiferal genera and their classification. – Vols. 1 and 2, 970 pp., 847 Pls., New York (Van Nostrand Reinhold).
Lohmann, K.C., 1988. Geochemical patterns of meteoric diagenetic systems and their application to studies of paleokarst. In: James, N.P., Choquette, P.W. (Eds.), Paleokarst. Springer, New York, pp. 58–80.
Mancinelli, A., Chiocchini, M., Chiocchini, R.A., Romano, A., 2005. Biostratigraphy of Upper Triassic-lower Jurassic carbonate platform sediments of the central-southern Apennines (Italy). Riv. Ital. Paleontol. Stratigr. 111, 271–283.
Marshall, J.D., 1992. Climatic and oceanographic isotopic signals from the carbonate rock record and their preservation. Geol. Mag. 129, 143–160.
Martindale, R.C., Berelson, W.M., Corsetti, F.A., Bottjer, D.J., West, A.J., 2012. Constraining carbonate chemistry at a potential ocean acidification event (the Triassic–Jurassic boundary) using the presence of corals and coral reefs in the fossil record. Palaeogeogr. Palaeoclimatol. Palaeoecol. 350, 114–123.
Martini, R., Vachard, D., Zaninetti, L., Cirilli, S., Cornée, J.J., Lathuilière, B., Villeneuve, M., 1997. Sedimentology, stratigraphy, and micropalaeontology of the Upper Triassic reefal series in Eastern Sulawesi (Indonesia). Palaeogeogr. Palaeoclimatol. Palaeoecol. 128, 157–174.
Marzoli, A., Renne, P.R., Piccirillo, E.M., Ernesto, M., Bellieni, G., Min, A.D., 1999. Extensive 200-million-year-old continental flood basalts of the Central Atlantic Magmatic Province. Science 284, 616–618.
Marzoli, A., Callegaro, S., Dal Corso, J., Davies, J.H., Chiaradia, M., Youbi, N., Bertrand, H., Reisberg, L., Merle, R., Jourdan, F., 2018. The Central Atlantic magmatic province (CAMP): A review. In: Tanner, L.H. (Ed.), The Late Triassic World. Springer, pp. 91–125.
Maurer, F., Rettori, R., Martini, R., 2008. Triassic stratigraphy, facies and evolution of the Arabian shelf in the northern United Arab Emirates. Int. J. Earth Sci. 97, 765–784.
Maurer, F., Krystyn, L., Martini, R., McRoberts, C., Rettori, R., Hofmann, P., 2015. Towards a refined Arabian Plate Triassic stratigraphy: insights from the Musandam Peninsula. 5th Arabian Plate Geology Workshop Lower Triassic to Middle Jurassic Evaporite-Carbonates-Siliciclastic Systems of the Arabian Plate (Sudair to Dhruma and Time Equivalent), (Abstract P05 and Poster, Kuwait).
McRoberts, C.A., Furrer, H., Jones, D.S., 1997. Palaeoenvironmental interpretation of a Triassic-Jurassic boundary section from Western Austria based on palaeoecological and geochemical data. Palaeogeogr. Palaeoclimatol. Palaeoecol. 136, 79–95.
McRoberts, C.A., Krystyn, L., Hautmann, M., 2012. Macrofaunal response to the end-Triassic mass extinction in the West-Tethyan Kössen Basin, Austria. Palaios 27, 607–616.
Mette, W., Thibault, N., Krystyn, L., Korte, C., Clémence, M.E., Ruhl, M., Rizzi, M., Ullmann, C.V., 2016. Rhaetian (Late Triassic) Biotic and Carbon Isotope Events and Intraplatform Basin Development in the Northern Calcareous Alps, Tyrol, Austria (Field trip 11, Geo. Alp., 233-256).
Ogg, J.G., Chen, Z.Q., Orchard, M.J., Jiang, H.S., 2020. The Triassic Period. In: Gradstein, et al. (Eds.), Geologic Time Scale 2020. Elsevier, Amsterdam, pp. 903–953.
Pálfy, J., Kovács, Z., Demény, A., Vallner, Z., 2021. End-Triassic crisis and "unreefing" led to the demise of the Dachstein carbonate platform: a revised model and evidence from the Transdanubian Range, Hungary. Global Planet. Change 199, 103428.
Parente, M., Amodio, S., Iannace, A., Sabbatino, M., 2022. Stratigraphy and facies of the Apennine Carbonate Platform (southern Italy): the record of Mesozoic OAEs and Miocene transgression. Geol. Field Trips Maps 14 (2.3), 1–74.
Patterson, W.P., Walter, L.M., 1994. Depletion of ^{13}C in seawater ΣCO_2 on modern carbonate platforms: significance for the carbon isotopic record of carbonates. Geology 22, 885–888.
Piller, W., 1978. Involutinacea (Foraminifera) der Trias und des Lias. Beiträge Paläont. Österreich, Wien 5, 1–164.
Prokoph, A., Shields, G.A., Veizer, J., 2008. Compilation and time-series analysis of a marine carbonate $\delta^{18}O$, $\delta^{13}C$, $^{87}Sr/^{86}Sr$ and $\delta^{34}S$ database through Earth history. Earth Sci. Rev. 87, 113–133.
Raup, D.M., Sepkoski Jr., J.J., 1982. Mass extinctions in the marine fossil record. Science 215, 1501–1503.
Reijmer, J.J., Everaars, J.S., 1991. Carbonate platform facies reflected in carbonate basin facies (Triassic, Northern Calcareous Alps, Austria). Facies 25, 253–277.
Rigaud, S., Martini, R., Rettori, R., 2012a. A new genus of Norian involutinid foraminifers: its morphological, biostratigraphic, and evolutionary significance. Acta Palaeontol. Pol. 58, 391–405.
Rigaud, S., Martini, R., Rettori, R., 2012b. Parvalamellinae, a new subfamily for Triassic glomospiroid Involutinidae. J. Foraminifer. Res. 42, 245–256.
Rigaud, S., Blau, J., Martini, R., Rettori, R., 2013. Taxonomy and phylogeny of the Trocholinidae (Involutinina). J. Foraminifer. Res. 43, 317–339.
Rigaud, S., Blau, J., Martini, R., Rettori, R., 2015. Taxonomy, phylogeny, and functional morphology of the foraminiferal genus *Involutina*. Acta Palaeontol. Pol. 60, 235–244.
Romano, R., Masetti, D., Carras, N., Barattolo, F., Roghi, G., 2008. The Triassic/Jurassic boundary in a peritidal carbonate platform of the Pelagonian domain: the Mount Messapion section (Chalkida, Greece). Riv. Ital. Paleontol. Stratigr. 114, 431–452.
Ruhl, M., Kürschner, W.M., 2011. Multiple phases of carbon cycle disturbance from large Igneous Province formation at the Triassic-Jurassic transition. Geology 39, 431–434.
Ruhl, M., Hesselbo, S.P., Al-Suwaidi, A., Jenkyns, H.C., Damborenea, S.E., Manceñido, M.O., Storm, M., Mather, T.A., Riccardi, A.C., 2020. On the onset of Central Atlantic Magmatic Province (CAMP) volcanism and environmental and carbon-cycle change at the Triassic–Jurassic transition (Neuquén Basin, Argentina). Earth Sci. Rev. 208, 103229.
Sartoni, S., Crescenti, U., 1962. Ricerche biostratigrafiche nel Mesozoico dell'Appennino meridionale. Giornale di Geologia, Serie 2°, 29, 161–293.
Schäfer, P., Senowbari-Daryan, B., 1981. Facies Development and Paleoecologic Zonation of four Upper Triassic Patch Reefs Northern Calcareous Alps near Salzburg Austria. SEPM Special Publications 30, 241–259.
Schoepfer, S.D., Algeo, T.J., van de Schootbrugge, B., Whiteside, J.H., 2022. The Triassic–Jurassic transition–A review of environmental change at the dawn of modern life. Earth Sci. Rev. 104099.
Septfontaine, M., 1984. Biozonation (a l'aide des foraminifères imperforés) de la Plate-forme interne carbonatée liasique du Haut Atlas (Maroc). Rev. Micropaleontol. 27, 209–229.
Skelton, P.W., Gili, E., 2012. Rudists and carbonate platforms in the Aptian: a case study on biotic interactions with ocean chemistry and climate. Sedimentology 59, 81–117.
Swart, P.K., 2011. Is there really a mixing-zone stable carbon and oxygen isotope signal. In: Abstracts, 28th IAS meeting of sedimentology, Zaragoza, Spain, 5-8 July 2011.
Tappan, H., Loeblich Jr., A.R., 1988. Foraminiferal evolution, diversification, and extinction. J. Paleontol. 62, 695–714.
Tassi, F., Bonini, M., Montegrossi, G., Capecchiacci, F., Capaccioni, B., Vaselli, O., 2012. Origin of light hydrocarbons in gases from mud volcanoes and CH_4-rich emissions. Chem. Geol. 294, 113–126.
Tavani, S., Granado, P., Corradetti, A., Camanni, G., Vignaroli, G., Manatschal, G., Mazzoli, S., Muñoz, J.A., Parente, M., 2021. Rift inheritance controls the switch from thin-to thick-skinned thrusting and basal décollement re-localization at the subduction-to-collision transition. GSA Bull. 133, 2157–2170.
Todaro, S., Di Stefano, P., Zarcone, G., Randazzo, V., 2017. Facies stacking and extinctions across the Triassic–Jurassic boundary in a peritidal succession from western Sicily. Facies 63, 1–21.
Todaro, S., Rigo, M., Randazzo, V., Di Stefano, P., 2018. The end-Triassic mass extinction: a new correlation between extinction events and $\delta^{13}C$ fluctuations from a Triassic-Jurassic peritidal succession in western Sicily. Sediment. Geol. 368, 105–113.
Todaro, S., Rigo, M., Stefano, P.D., Aiuppa, A., Chiaradia, M., 2022. End-Triassic Extinction in a carbonate platform from Western Tethys: a comparison between extinction trends and geochemical variations. Front. Earth Sci. 10, 875466.
Trecalli, A., Spangenberg, J., Adatte, T., Föllmi, K.B., Parente, M., 2012. Carbonate platform evidence of ocean acidification at the onset of the early Toarcian oceanic anoxic event. Earth Planet. Sci. Lett. 357, 214–225.
Urban, I., Demangel, I., Krystyn, L., Calner, M., Kovács, Z., Gradwohl, G., Lernpeiss, S., Maurer, F., Richoz, S., 2023. Mid-Norian to Hettangian record and time-specific oolites during the end-Triassic Mass Extinction at Wadi Milaha, Musandam Peninsula, United Arab Emirates. J. Asian Earth Sci. 9, 100138.
Vasconcelos, C., McKenzie, J.A., Warthmann, R., Bernasconi, S.M., 2005. Calibration of the $\delta^{18}O$ paleothermometer for dolomite precipitated in microbial cultures and natural environments. Geology 33 (4), 317–320.
Velić, I., 2007. Stratigraphy and palaeobiogeography of Mesozoic benthic foraminifera of the Karst Dinarides (SE Europe)-part 1. Geologia Croatica 60, 1–60.
Weber, J.N., Woodhead, P.M., 1969. Factors affecting the carbon and oxygen isotopic composition of marine carbonate sediments II. Heron Island, Great Barrier Reef, Australia. Geochim. Cosmochim. Acta 33, 19–38.
Weissert, H., Lini, A., Föllmi, K.B., Kuhn, O., 1998. Correlation of early cretaceous carbon isotope stratigraphy and platform drowning events: a possible link? Palaeogeogr. Palaeoclimatol. Palaeoecol. 137, 189–203.
West, R.R., 2015. Paleogeography and Biostratigraphy of the hypercacified chaetetid-type Porifera (Demospongiae). In: Treatise on Invertebrate Paleontology. Part E. (Revised) Porifera. Hypercalcified Porifera. The University of Kansas Paleontological Institute Lawrence, Selden, PA, pp. 179–191.
Whiteside, J.H., Olsen, P.E., Eglinton, T., Brookfield, M.E., Sambrotto, R.N., 2010. Compound-specific carbon isotopes from Earth's largest flood basalt eruptions directly linked to the end-Triassic mass extinction. Proc. Natl. Acad. Sci. 107, 6721–6725.
Wignall, P.B., Atkinson, J.W., 2020. A Two-phase End-Triassic Mass Extinction. Earth Sci. Rev. 208, 103282.
Zaffani, M., Jadoul, F., Rigo, M., 2018. A new Rhaetian $\delta^{13}C_{org}$ record: carbon cycle disturbances, volcanism, End-Triassic Mass Extinction (ETE). Earth Sci. Rev. 178, 92–104.
Zaninetti, L., Martini, R., Dumont, T., 1992. Triassic foraminifers from Sites 761 and 764, Wombat Plateau, Northwest Australia, in von Rad, U., Haq, B.U., et al., Proceedings of the Ocean Drilling Program, Scientific Results Volume 122: College Station, Texas, 122, pp. 427–436.
Zarcone, G., Petti, F.M., Cillari, A., Di Stefano, P., Guzzetta, D., Nicosia, U., 2010. A possible bridge between Adria and Africa: new palaeobiogeographic and stratigraphic constraints on the Mesozoic palaeogeography of the Central Mediterranean area. Earth Sci. Rev. 103, 154–162.